

Approved
Contrails
X AFFDL-TR-65-161

PART I

GENERAL INSTABILITY OF ORTHOTROPICALLY STIFFENED CYLINDERS

PART II

BENDING AND COMBINED
COMPRESSION AND BENDING

C. LAKSHMIKANTHAM
GEORGE GERARD
ROGER MILLIGAN

14-00000-1000
TECHNICAL REPORT AFFDL TR 65 161, PART II
AUGUST 1965

AIR FORCE FLIGHT DYNAMICS LABORATORY
RESEARCH AND TECHNOLOGY DIVISION
AIR FORCE SYSTEMS COMMAND
UNITED STATES AIR FORCE
WRIGHT PATTERSON AIR FORCE BASE, OHIO

DISTRIBUTION OF THIS DOCUMENT IS UNLIMITED

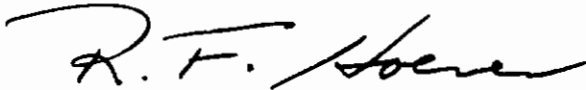
FOREWORD

This report was prepared by Allied Research Associates, Inc., Concord, Massachusetts, under USAF Contract No. AF 33(615)-1228. The contract was initiated under Project Nr. 1467, Task Nr. 146703 BPSN 4 (6199-146703-62405334). The work was administered under the direction of the Air Force Flight Dynamics Laboratory, Research and Technology Division, Messrs. Abel Abdessalam and Royce Forman, FDTR, project engineers.

This report covers work conducted on this phase from November 1963 to June 1965.

The work was performed in the ARA Division of Allied Research Associates, Inc. and the Allied report number is ARA Technical Report No. 258-3.

This technical report has been received and is approved.



RICHARD F. HOENER
Acting Chief
Structures Division

ABSTRACT

As part of a general program to determine the applicability of linear orthotropic theory to the design of cylindrical shells under various loading conditions, a theoretical and experimental investigation was performed on the general instability of orthotropic cylinders under bending and combined axial compression and bending loading.

Based on a simple approximation for the asymmetric buckling pattern, theoretical results suitable for design use were obtained for the buckling of orthotropic cylinders for both bending and combined loading conditions. It was shown that the buckling stress for orthotropic cylinders under bending or axial compression loading are equal which agrees with previous results for isotropic cylinders. Theoretical results were evaluated by means of a series of careful experiments performed on orthotropically stiffened cylinders designed to fail in the elastic general instability mode. For both bending loading and the combined axial and bending loading condition, experimental results were in good agreement with the theory.

TABLE OF CONTENTS

	PAGE	
SYMBOLS	v	
SECTION 1	INTRODUCTION	1
SECTION 2	CORRELATION OF THEORY AND EXPERIMENTAL RESULTS	2
	Bending	2
	Combined Compression and Bending	2
SECTION 3	BENDING ELASTIC STABILITY OF ISOTROPIC CYLINDERS	5
	Governing Equations	6
	Bending Solution	8
	Buckle Wavelengths	10
	The Effect of Bending on Compression	11
	Concluding Remarks	12
SECTION 4	BENDING ELASTIC STABILITY OF ORTHOTROPIC CYLINDERS	13
	Governing Equations	13
	Buckling Mode	15
	Bending Solution	15
	m-continuous Solution	17
	Limiting Solution	18
	m=1 Solution	19
	Comparison of Solutions	19
	Compressive Stability	23
	Comparison of Bending and Compressive Stability	24
	Concluding Remarks	24
SECTION 5	BENDING TESTS	25
	Design and Fabrication of Test Specimens	25
	Test Arrangement and Procedure	25
	Accuracy of Experimental Data	27
	Reduction of Test Data on Failure of Cylinders	30
	Calculation of Theoretical Structural Parameters	31
SECTION 6	COMBINED LOADING TESTS	35
	Design and Fabrication of Test Specimens	35
	Test Arrangement and Procedure	35
	Accuracy of Experimental Data	35
	Reduction of Test Data on Failure of Cylinders	37
	Calculation of Theoretical Structural Parameters	38
	Calculation of Stress Ratios	38
REFERENCES		41

LIST OF SYMBOLS

B_1, B_2, B_3	axial rigidities for the orthotropic cylinder
C	test machine calibration factor
D_1, D_2, D_3	bending rigidities for the orthotropic cylinder
E	Young's modulus
F	stress function
F_x	Equation (59)
I_f	area moment of inertia of skin and stiffener per unit width in a plane perpendicular to circumferential direction
I_s	area moment of inertia of skin and stiffener per unit width in a plane perpendicular to the longitudinal direction
J	torsional moment of inertia per unit width
L	cylinder length
M	external applied moment
M_{exp}	experimental bending moment
M_b	theoretical bending moment
$M_\theta, M_x, M_{x\theta}$	bending stress resultants
\bar{N}_b, \bar{N}_c	constant axial forces for the bending and compressive problems
$N_\theta, N_x, N_{x\theta}$	membrane stress resultants
P_{exp}	experimental axial compressive load
R	radius of the cylinder
Z	curvature parameter given by $Z = \frac{L^2}{Rt}(1 - \nu^2)^{1/2}$ for the isotropic case and by $Z^2 = B_2 L^4 / 12 R^2 D_1$ for the orthotropic case
Z_x	orthotropic cylinder curvature parameter (Eq. 62)
b	stiffener height
c	curvature parameter defined by $c^2 = 12(1 - \nu^2) / R^2 t^2$
d	stiffener spacing
d_f	stiffener spacing in longitudinal direction
d_s	stiffener spacing in circumferential direction

List of Symbols (Continued)

$k_{b\text{exp}}$	experimental buckling coefficient in bending
k_x	cylinder buckling coefficient
p_{exp}	test machine pressure loading at specimen failure
t	cylinder wall thickness
\bar{t}	effective shear thickness of cylinder cross section
t_f	area of sheet and stiffener per unit width in a plane perpendicular to the circumferential direction
t_s	area of sheet and stiffener per unit width in a plane perpendicular to the longitudinal direction.
u, v, w	displacement in axial, circumferential and normal directions
w	stiffener width
w_f	stiffener width in longitudinal direction
w_s	stiffener width in circumferential direction
x, θ	axial and circumferential coordinates
α	orthotropicity parameter = $B_1 D_2 / B_2 D_1$
β^*, β	wavelength parameters for the bending and compressive cases
$\bar{\beta}^*, \bar{\beta}$	weighted wavelength parameters for the bending and compressive cases
γ	orthotropicity parameter defined in Eq. (40)
δ	orthotropicity parameter defined in Eq. (40)
$\epsilon_x, \epsilon_\theta, \epsilon_{x\theta}$	axial strain variations
λ^*, λ	axial wavelengths for the bending and compressive cases
ν	Poisson's ratio
σ_b	bending stress
$\sigma_{b\text{exp}}$	experimental bending stress
σ_x	theoretical cylinder buckling stress under either axial compression or bending loading
τ	ratio of bending to compressive forces at buckling
$\chi_x, \chi_\theta, \chi_{x\theta}$	curvature changes of middle surface
∇_B^4, \square^4	linear operators given in Eqs. (27) and (29)

GENERAL INSTABILITY OF ORTHOTROPICALLY
STIFFENED CYLINDERS

PART II. BENDING AND COMBINED COMPRESSION AND BENDING

SECTION I
INTRODUCTION

The major objective of the program described herein is to conduct a series of careful experiments on elastic general instability of orthotropically stiffened cylinders under a variety of loadings and correlate the experimental data with theory. Part I of this program involved a rather extensive series of tests on longitudinal, ring, and grid stiffened cylinders under axial compression, torsion, and hydrostatic pressure. The correlation of these data with available theory, as well as the experimental details, are reported in Ref. 1.

For orthotropically stiffened cylinders under bending or under combined compression and bending, no satisfactory theory was available at the start of this program. As a consequence, a major portion of this phase of the program was devoted to the development of a linear orthotropic theory for cylindrical shells under bending and combined compression and bending. In addition, a representative series of tests were conducted on longitudinal, ring and grid stiffened cylinders under bending. Finally, several tests were conducted for combined compression and bending on longitudinal and ring stiffened cylinders.

This report is thus devoted to the bending phase of the program. Section 2 essentially summarizes the significant results by presenting a correlation of the experimental results with the theory. In general, excellent correlation with linear orthotropic theory is obtained for the range of variables tested.

The theoretical development is contained in Secs. 3 and 4. A satisfactory solution for the elastic bending stability of an isotropic cylinder has been obtained only recently by Seide and Weingarten in Ref. 2. Their solution requires tedious calculations which if applied to orthotropically stiffened cylinders would introduce great complexities. As a consequence, Sec. 3 is devoted to a relatively simple although highly accurate approximation of the isotropic cylinder solution, which is substantiated by the results of Ref. 2. This approximation is then utilized in considering combined compression and bending of an isotropic cylinder in Sec. 3 and elastic general instability of orthotropic cylinders under bending in Sec. 4.

The experimental details of the tests conducted on longitudinal, ring and grid stiffened cylinders under bending, and combined compression and bending are presented in Secs. 5 and 6, respectively.

SECTION 2 CORRELATION OF THEORY AND EXPERIMENTAL RESULTS

All cylinders tested in this program were designed to fail in the elastic general instability mode. They were very carefully machined of 6061-T6 aluminum alloy with closely spaced integral longitudinal, ring or grid stiffening systems to form nominally 8 inch diameter orthotropic cylinders. They were carefully tested in specially designed testing machines which utilized pneumatic loading systems in all cases.

Bending

The specimens tested in bending were generally counterparts of those tested under axial compression (Ref. 1) in that corresponding values of α and γ were utilized. The correlation of general instability theory and test data for the stiffened cylinders under bending is illustrated in Fig. 1. The theoretical buckling mode for the ring and grid stiffened cylinders is axisymmetric, whereas for the longitudinal stiffened cylinders it is the $m = 1$ asymmetric mode.

It can be observed from Fig. 1 that the experimental data are in good agreement with the predictions of linear orthotropic stability theory over the rather broad range of α covered by the test data. Similar agreement was obtained in Ref. 1 for the stiffened cylinders under compressive loads. A comparison of the set of data for bending with that for compression indicates that there is no difference in the critical compressive loading for the two cases either theoretically or experimentally.

Combined Compression and Bending

The theory developed herein for cylinders under combined compression and bending indicates a linear interaction relationship as shown in Fig. 2. Combined load test data for a longitudinally stiffened cylinder of $\alpha = 0.11$ and a ring stiffened cylinder of $\alpha = 1.6$ are shown in Fig. 2 in conjunction with corresponding test data for the individual loading cases. It is to be noted that in all cases, the stress ratio (R) represents the experimental to theoretical stress ratio for the specific specimen configuration.

A comparison of the test data with the linear interaction theory indicates substantially good correlation. These results, in conjunction with those obtained under bending only, substantiate the theoretical conclusion that general instability occurs when the critical compressive loading is exceeded in any region of the cylinder cross section.

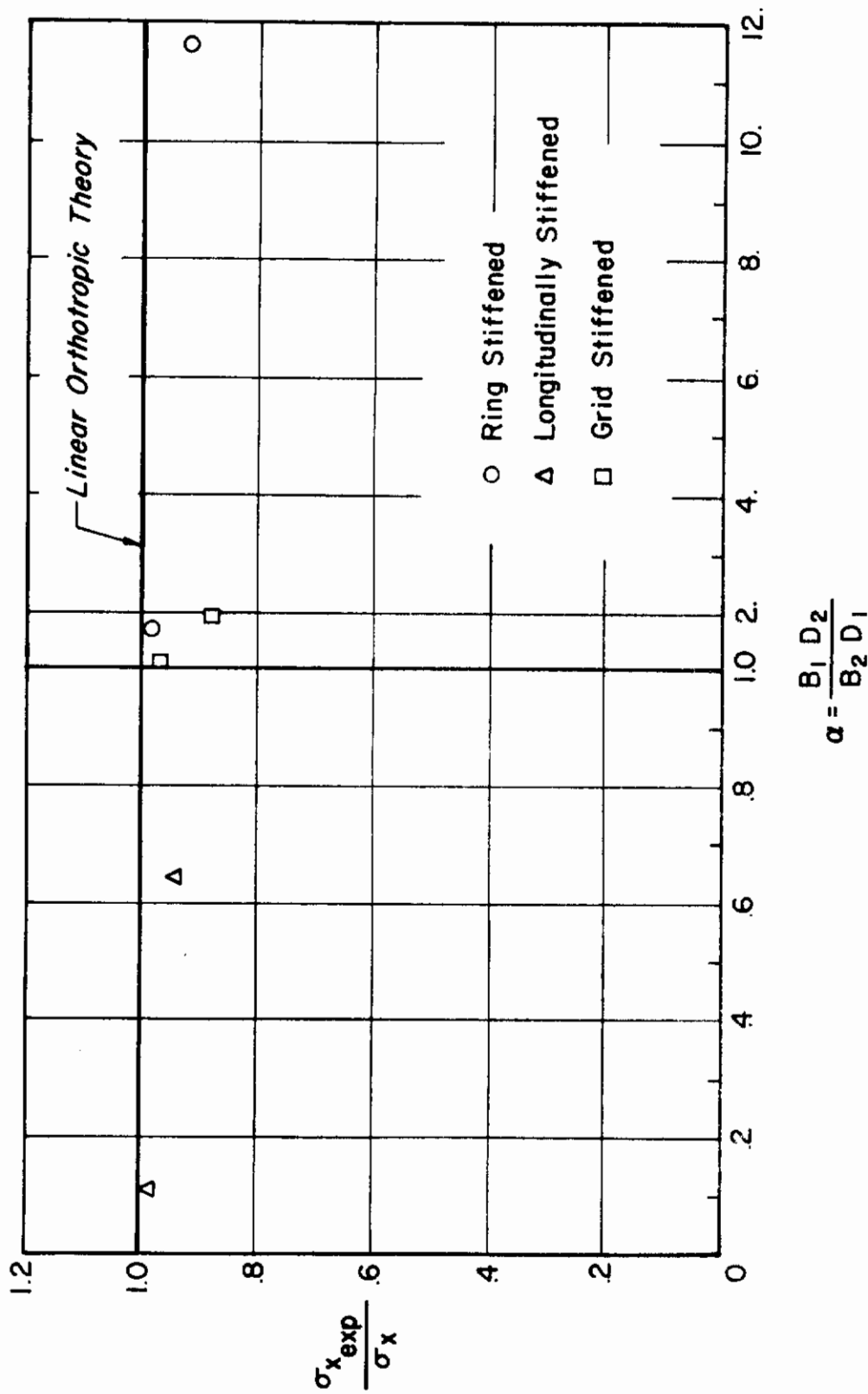


Fig. 1. Correlation of Theory and Experiments for Orthotropic Cylinders In Bending.

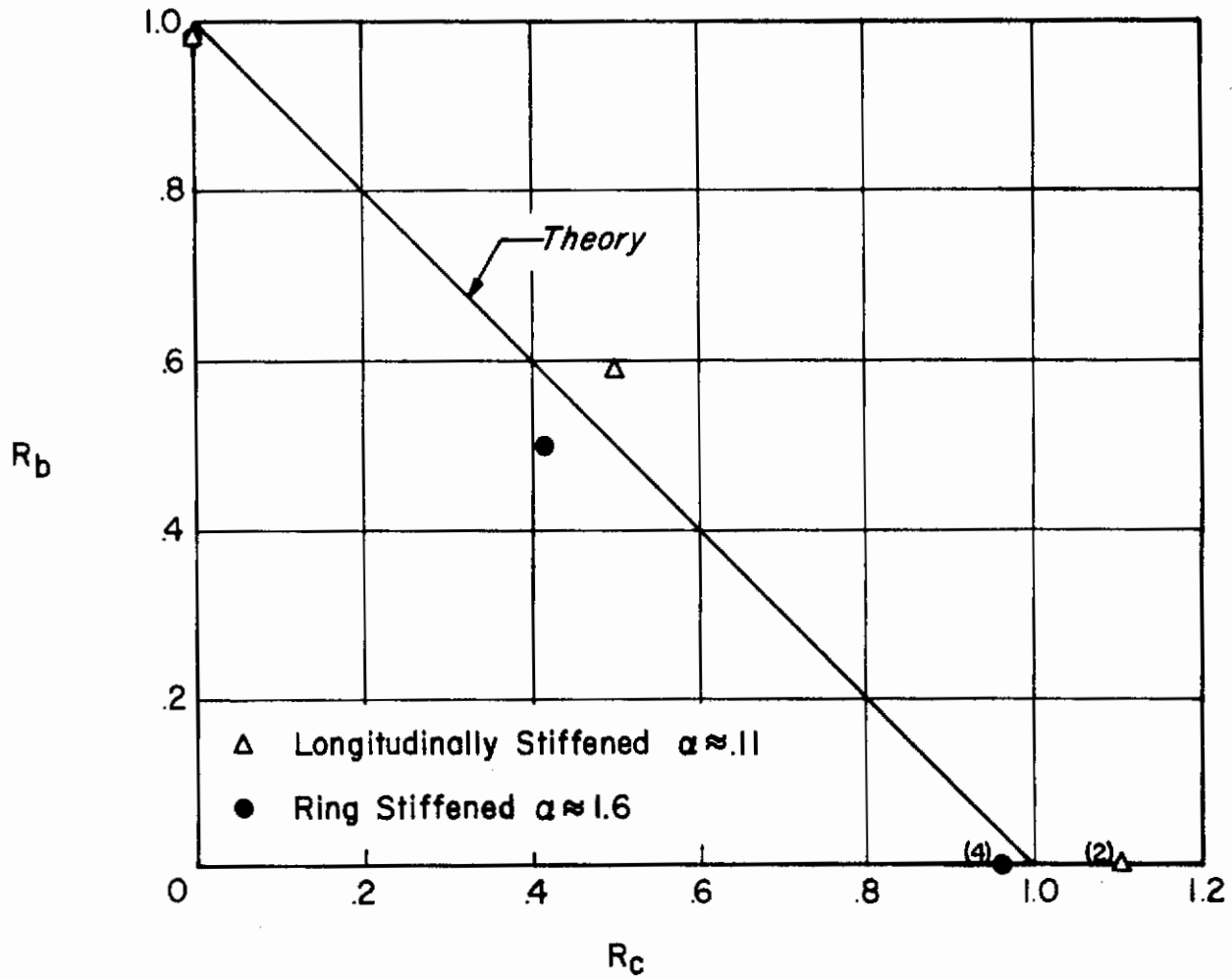


Fig. 2. Combined Loading Interaction Curve.

SECTION 3
BENDING ELASTIC STABILITY OF ISOTROPIC CYLINDERS

The bending stability problem of isotropic cylinders has interested only a few workers in the past and only recently Seide and Weingarten (Ref. 2) have shown conclusively that in isotropic cylinders, the critical stress for bending stability is essentially the same as that in the corresponding compressive stability problem though the buckle pattern is quite different.

While Ref. 2 deals mainly with the establishment of the critical stress results, the deflection pattern obtained for the buckles as a result of elaborate computations presents certain interesting features. The dominant feature is that the buckle pattern is an asymmetric one, since any axisymmetric mode is incompatible with the bending problem. While this has no great significance in the isotropic case, it is of considerable importance in the orthotropic case, especially in the light of the compressive stability of such cylinders studied by Gerard (Ref. 3).

A simple approximate representation of the Seide and Weingarten buckle pattern developed in this section for isotropic cylinders yields results for the critical stresses quite readily and furthermore throws some light on the role of the buckle pattern upon the ratio of critical stresses. The isotropic case is presented as a prelude to the orthotropic case which is considered in Sec. 4. Further, an insight is obtained into the incipient buckling geometry when compressive loads are combined with bending loads for an isotropic cylinder.

Governing Equations

The governing equation for the stability of an isotropic cylinder under an externally applied bending moment M , is given as follows (Ref. 2);

$$L(w) \equiv D \nabla^4 w + \bar{N}_x \frac{\partial^2 w}{\partial x^2} + \frac{Et}{R^2} \nabla^{-4} \frac{\partial^4 w}{\partial x^4} = 0 \quad (1)$$

where \bar{N}_x is the equivalent axial force. If the problem were one of pure compression $\bar{N}_x = \bar{N}_c = P/2\pi R$, where P would signify the compressive load. However, for pure bending, $\bar{N}_x = \bar{N}_b \cos \theta$ where $\bar{N}_b = M/\pi R^2$, the maximum fiber stress resultant occurring at the top of the cylinder. In Eq. (1), ∇^{-4} is the inverse operator given by

$$\nabla^{-4} (\nabla^4 w) = w \quad (2)$$

Since Eq. (1) cannot be solved exactly for the pure bending case, that is $\bar{N}_x = \bar{N}_b \cos \theta$, the Galerkin method is used with the following series assumed for w :

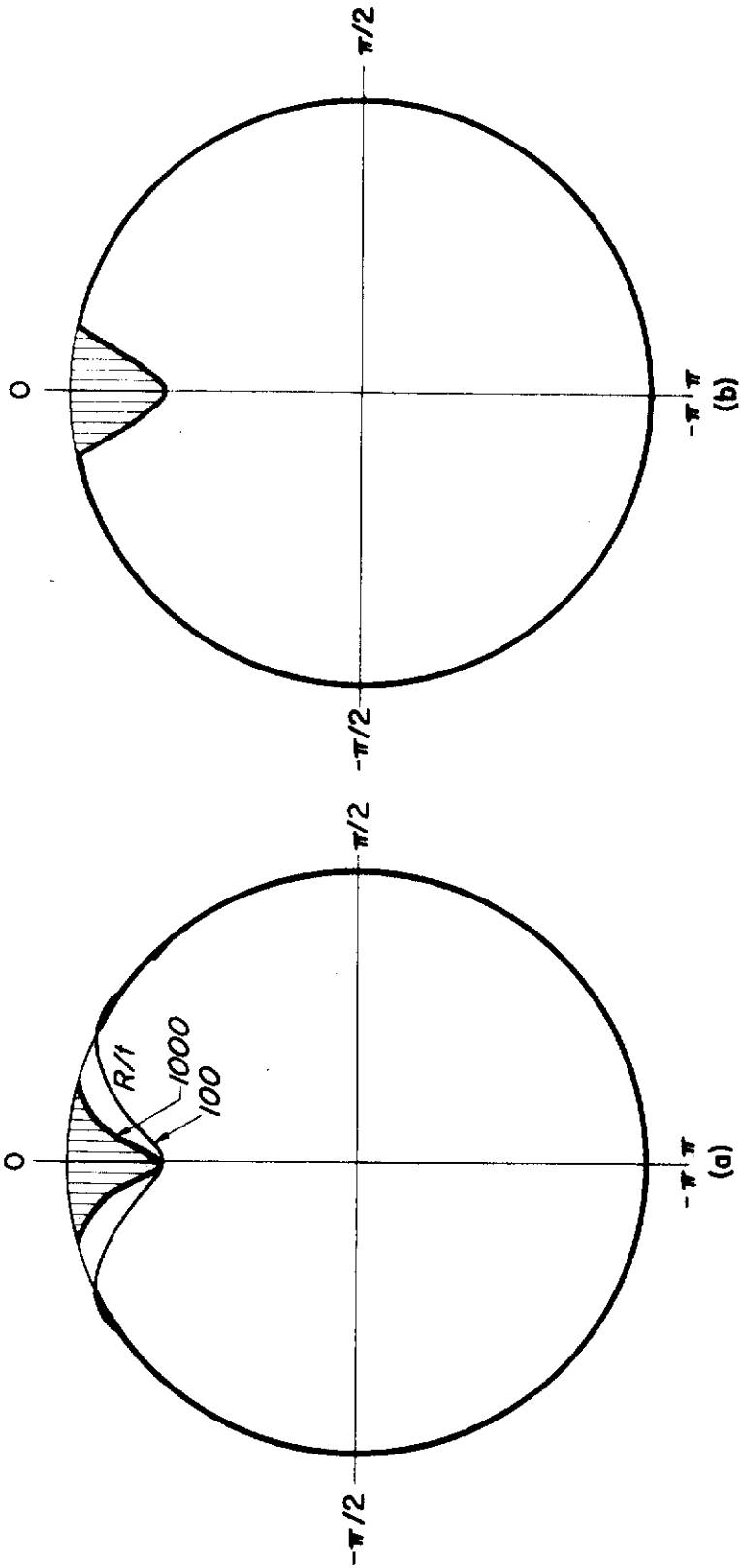
$$w = \sin(x/\lambda_x^*) \sum_{n=0}^{\infty} a_n \cos n \theta \quad (3)$$

where the star denotes conditions for pure bending.

The Galerkin equations for the coefficients a_n are obtained by substituting Eq. (3) into Eq. (1), and setting,

$$\int_0^L \int_0^{2\pi} [L(w) \sin(x/\lambda_x^*) \sum_{n=0}^{\infty} \cos n \theta] R d\theta dx = 0 \quad (4)$$

Eq. (4) yields an infinite system of linear homogeneous equations and the stability criterion is given by the vanishing of the determinant. The size of the determinant is varied until the lowest eigenvalue is obtained to the desired accuracy. By taking as many as 50 terms for certain R/t ratios, Seide and Weingarten obtained the result that the bending/compression critical stress ratio approaches the minimum value of unity. The shape of the deflection function obtained by them for various R/t values is reproduced in Figure 3a.



$$w = A \sin \left(X / \lambda_x^* \right) \cos N \theta \quad |\theta| \leq \pi/2N$$

$$w = 0 \quad \text{for } \theta \text{ elsewhere}$$

APPROXIMATION OF THIS REPORT

$$w = \sum \sigma_n \sin \left(X / \lambda_x \right) \cos n \theta$$

SEIDE & WEINGARTEN
SOLUTION

Fig. 3. Asymmetric Buckle Pattern for Isotropic Cylinders and Its Approximation.

The deflection function is seen to behave like a highly damped wave symmetrical about the vertical diameter consisting essentially of a single lobe whose maximum half width is not greater than about 22.5° for the highest R/t ratio.

Hence the Seide and Weingarten buckle pattern may be approximated by the following analytical expression:

$$w = A \sin(x/\lambda_x^*) \cos N\theta \quad \text{for } |\theta| \leq \pi/2N \quad (5)$$

$$= 0 \text{ elsewhere on the circumference}$$

N being a fixed number ≥ 1 .

The above analytical expression corresponds to a single lobe, which is shown in Figure 3b.

Bending Solution

Eq. (5) corresponds to a one term approximation to the series, Eq. (3). The least half width of the lobe in Figure 3a would correspond to $N = 4$, and the greatest, to $N = 6$. Using Eq. (5) in Eq. (1) we obtain from the Galerkin equation,

$$\int_0^L \int_{-\pi/2N}^{\pi/2N} L(w) \sin(x/\lambda_x^*) \cos N\theta \, d\theta \, dx = 0 \quad (6)$$

the following expression for the bending force \overline{N}_b :

$$\frac{\overline{N}_b}{D} = \frac{\pi/2N}{\sin(\pi/2N)} \left(1 - \frac{1}{4N^2}\right) \left[\frac{c^2 \lambda_x^{*2}}{(1 + N^2 \lambda_x^{*2}/R^2)^2} + \frac{(1 + N^2 \lambda_x^{*2}/R^2)^2}{\lambda_x^{*2}} \right] \quad (7)$$

where $c^2 = 12(1 - \nu^2)/R^2 t^2$.

The minimum value of the expression in the square brackets which is of the form $(Au + 1/u)$, is seen to be equal to $2c$ from which we may write for a moderate length cylinder:

$$(\overline{N}_b/D)_{\min} = 2c \frac{\pi/2N}{\sin \pi/2N} \left(1 - \frac{1}{4N^2}\right)$$

or

$$k_b = 0.702 Z \frac{\pi/2N}{\sin \pi/2N} \left(1 - \frac{1}{4N^2}\right) \quad (8)$$

where

$$k_b = \frac{\bar{N}_b L^2}{\pi^2 D}; Z = \frac{L^2}{Rt} (1 - \nu^2)^{\frac{1}{2}}$$

Now, the classical compressive buckling coefficient for a moderate length cylinder, k_c , bears the well known relation to Z given by:

$$k_c = 0.702 Z$$

Then from Eq. (8) we find

$$k_b/k_c = \frac{\pi/2N}{\sin(\pi/2N)} \left(1 - \frac{1}{4N^2}\right) \quad (9)$$

The ratio k_b/k_c is seen to approach unity as N becomes large; thus with $N = 6$, $k_b/k_c = 1.005$. This value of N corresponds to a lobe width of 15° and the k_b/k_c value is seen to agree with the result for $500 < R/t < 1000$ in Ref. 2. Similarly $N = 4$ ($k_b/k_c = 1.01$) agrees with the result for $R/t = 200$ therein.

For moderate length cylinders, $N \geq 4$ would seem to be a reasonable assumption to make, and hence one can assume that the expression $[(\pi/2N)/\sin(\pi/2N)](1 - 1/4N^2)$ is approximately equal to unity in further considerations. Hence we can write Eq. (7) as:

$$\frac{\bar{N}_b}{D} \approx \frac{c^2 \lambda_x^{*2}}{(1 + N^2 \lambda_x^{*2}/R^2)^2} + \frac{(1 + N^2 \lambda_x^{*2}/R^2)^2}{\lambda_x^{*2}} \quad (10)$$

From Eq. (10) we establish the Seide and Weingarten result for the stress ratios quite easily.

It is interesting to examine the result of including more lobes in the deflection model and ultimately letting them occur all along the top half of the cylinder circumference. Suppose Eq. (5) is valid for $|\theta| \leq 3\pi/2N$, $N \geq 3$ and $w = 0$ elsewhere. Then, corresponding to Eq. (9), we would obtain

$$k_b/k_c = \frac{3\pi/2N}{\sin 3\pi/2N} \left(1 - \frac{1}{4N^2}\right) \quad (11)$$

It is clear that for the same N (≥ 3) Eq. (11) yields a higher value for k_b/k_c than Eq. (9) which has one lobe, though ultimately as N becomes very large Eq. (11)

also yields $k_b/k_c = 1$. Thus it becomes evident that the single dimple state carries the least energy and hence offers the lowest value for k_b/k_c which is unity. This is the essential result for the cylinder in bending.

If the dimples occur all along the top half of the cylinder circumference and N is taken as large, in the limit we obtain that the value of $k_b/k_c = \pi/2$ which is an upper limit on the k_b/k_c ratio. Thus the formulation of Eq. (5) not only provides us with a ready verification of isotropic case, but also indicates that higher values of k_b/k_c occur with larger number of lobes. Since we are interested in the lowest value of the k_b/k_c ratio, it is evident that the single dimple corresponds to this case.

Buckle Wavelengths

At this stage it is interesting to examine the wavelength picture. Seide and Weingarten obtain an approximate expression for the wavelength in the axial direction for the pure bending case as follows:

$$\lambda_x^* \approx (Rt)^{\frac{1}{2}} / [12(1 - \nu^2)]^{\frac{1}{4}} \quad (12)$$

where the starred quantity denotes pure bending. In the corresponding pure compression case, if we were to examine the wavelength characteristic we find that the governing buckling mode can be axisymmetric or asymmetric. Thus if for w we take

$$w = A \sin(x/\lambda_x) \cos n\theta$$

we obtain from Eq. (1), taking $\bar{N}_x = \bar{N}_c$, the following expression:

$$\frac{\bar{N}_c}{D} = \frac{c^2 \lambda_x^2}{(1 + n^2 \lambda_x^2 / R^2)^2} + \frac{(1 + n^2 \lambda_x^2 / R^2)^2}{\lambda_x^2} \quad (13)$$

While Eqs. (13) and (10) bear resemblance, and a direct minimization yields in both cases the same result, namely $2c$, the wavelength picture is not necessarily the same. First, we notice that in Eq. (13) $n \geq 0$ whereas, in Eq. (10) $N \geq 4$. Thus while Eq. (13) gives rise to an axisymmetric mode, Eq. (10) definitely precludes this possibility. In Eq. (13) if the axisymmetric solution $n = 0$ is chosen, then the value of λ_x for minimum \bar{N}_c/D is evidently:

$$\lambda_x = (Rt)^{\frac{1}{2}} / [12(1 - \nu^2)]^{\frac{1}{4}} \quad (14)$$

which agrees with Eq (12) identically. Hence $\lambda_x = \lambda_x^*$. However, if in Eq. (13) $n > 0$, it is difficult to establish the result for λ_x . On the other hand, if $\lambda_x < \lambda_x^*$, it can be shown for $\bar{N}_c/D = 2c$ that $\beta = n\lambda_x/R$ is imaginary. Hence for all β real and > 0 , $\lambda_x > \lambda_x^*$.

Hence we find that generally the axial wavelength of pure bending less than the corresponding compressive case, i. e. ,

$$\lambda_x^* < \lambda_x \quad (15)$$

the equality holding for the value of λ_x corresponding to the axisymmetric mode.

Thus we find that as we change from the compression problem to the bending problem, though the critical stress has the same value, the wavelength as well as the buckle pattern is affected.

The Effect of Bending on Compression

This problem is of importance as it has definite bearing on experiments as usually some bending force is unavoidable in a compression test. Hence \bar{N}_b , the bending force is considered as a small constant force present along with \bar{N}_c the external compressive force. Using the same one lobe model considered in the pure bending case, that is, $w = A \sin(x/\lambda_x) \cos N\theta$, $|\theta| \leq \pi/2N$ and $w = 0$ elsewhere; with N as a large number, we obtain the following expression from the Galerkin equation.

$$\frac{N_c}{D} \frac{\pi}{2N} + \frac{N_b}{D} \sin \frac{\pi}{2N} \left(\frac{4N^2}{4N^2 - 1} \right) = \frac{\pi}{2N} \left[\frac{c^2 \lambda_x^2}{(1 + N^2 \lambda_x^2 / R^2)^2} + \frac{(1 + N^2 \lambda_x^2 / R^2)^2}{\lambda_x^2} \right] \quad (16)$$

Letting $\bar{N}_b/\bar{N}_c = \tau$ be a small fixed quantity, we obtain from Eq. (16):

$$\bar{N}_c/D = \frac{1}{1 + \tau \frac{\sin \pi/2N}{\pi/2N} \left(\frac{4N^2}{4N^2 - 1} \right)} \left[\frac{c^2 \lambda_x^2}{(1 + N^2 \lambda_x^2 / R^2)^2} + \frac{(1 + N^2 \lambda_x^2 / R^2)^2}{\lambda_x^2} \right] \quad (17)$$

and since N is assumed large, Eq. (17) yields

$$(\bar{N}_c/D)_{\min} = \frac{2c}{1 + \tau} \quad (18)$$

As in pure bending, we might increase the number of lobes, say to three. If $(\bar{N}_c/D)_{\min}^{(I)}$ denotes the value with one lobe, then

$$(\bar{N}_c/D)^{(III)} = \frac{2c}{1 + \tau \frac{\sin 3\pi/2N}{3\pi/2N} \left(\frac{4N^2}{4N^2 - 1} \right)}$$

Again as in the pure bending case we find

$$(\bar{N}_c/D)^I < (\bar{N}_c/D)^{III} \dots < (\bar{N}_c/D)^{(N)}$$

If we carry the lobes all along the top half we find in the limit

$$(\bar{N}_c/D)_{\min}^{(N)} = \frac{2c}{1 + \tau 2/\pi} \quad (19)$$

Thus the following interesting fact emerges from the above considerations: if there is any small bending present in a compression buckling, the buckle pattern, at least at the incipient stage of instability which is within the classical theory used herein, that has the least energy and hence the most likely one to occur is that with a single lobe in the cross sectional plane.

Concluding Remarks

The dominant feature that distinguishes the bending problem from the compression problem lies in the buckle pattern. In a compressive problem we have both axi- and asymmetric modes prevailing while in the bending problem a single lobe pattern in the cross sectional plane is the only one mode that is possible. Further the critical stress in both the bending and compressive problems is nearly the same. The present representation helps not only to establish the stress result in an elementary way, but also provides some insight into the instability in combined bending and compression of an isotropic cylinder of moderate length.

SECTION 4

BENDING ELASTIC STABILITY OF ORTHOTROPIC CYLINDERS

Governing Equations

Though the governing Donnell type equation for the elastic stability of orthotropic cylinders has been used by Taylor (Ref. 4), it will be advantageous to rederive it from a viewpoint of a consistent notation.

The middle surface strain and curvature variations are related to the displacements u , v and w , under the assumptions consistent with Donnell theory, as follows:

$$\begin{aligned} \epsilon_x &= \partial u / \partial x & \chi_x &= \partial^2 w / \partial x^2 \\ \epsilon_\theta &= (1/R) \partial v / \partial \theta + w/R & \chi_\theta &= (1/R^2) \partial^2 w / \partial \theta^2 \\ \epsilon_{x\theta} &= 1/2 [\partial v / \partial x + (1/R) \partial u / \partial \theta] & \chi_{x\theta} &= (1/R) \partial^2 w / \partial x \partial \theta \end{aligned} \quad (20)$$

The direct strain components ϵ_x , ϵ_θ , and $\epsilon_{x\theta}$ are seen to satisfy the following compatibility relationship:

$$\partial^2 \epsilon_\theta / \partial x^2 - (2/R) \partial^2 \epsilon_{x\theta} / \partial x \partial \theta + (1/R^2) \partial^2 \epsilon_x / \partial \theta^2 = (1/R) \partial^2 w / \partial x^2 \quad (21)$$

A set of equilibrium equations, consistent with the above strain field, may be written for the stress resultants during buckling under the action of a constant external equivalent axial force \bar{N}_x , defined in the same manner as for the isotropic cylinder:

$$\begin{aligned} \partial N_x / \partial x + (1/R) \partial N_{x\theta} / \partial \theta &= 0 \\ \partial N_{x\theta} / \partial x + (1/R) \partial N_\theta / \partial \theta &= 0 \end{aligned} \quad (22)$$

$$\partial^2 M_x / \partial x^2 + (2/R) \partial^2 M_{x\theta} / \partial x \partial \theta + 1/R^2 \partial^2 M_\theta / \partial \theta^2 + N_\theta / R + \bar{N}_x \partial^2 w / \partial x^2 = 0$$

The stress resultant - strain relationship for an orthotropic elastic material can be written as follows:

$$\begin{aligned} N_x &= B_1 (\epsilon_x + \nu \epsilon_\theta) & M_x &= D_1 (\chi_x + \nu \chi_\theta) \\ N_\theta &= B_2 (\epsilon_\theta + \nu \epsilon_x) & M_\theta &= D_2 (\chi_\theta + \nu \chi_x) \\ N_{x\theta} &= B_3 (1 - \nu) \epsilon_{x\theta} & M_{x\theta} &= D_3 (1 - \nu) \chi_{x\theta} \end{aligned} \quad (23)$$

where B_n and D_n , the axial and flexural rigidities are given by:

$$B_n = \frac{Et_n}{(1-\nu^2)} \quad D_n = \frac{EI_n}{(1-\nu^2)} \quad (n = 1, 2, 3) \quad (24)$$

The thicknesses t_1, t_2, t_3 are not necessarily physical thicknesses but generalized thicknesses, and I_1, I_2, I_3 are similarly generalized moments of inertia. In particular cases, as for instance in a monocoque construction with stringers, Taylor (Ref. 4), indicates the significance of these generalized thicknesses. A further discussion of these parameters is given by Becker and Gerard (Ref. 5).

The first two of the equilibrium equations, Eq. (22), are seen to be satisfied by the introduction of a stress function F , such that:

$$N_x = (1/R^2) \partial^2 F / \partial \theta^2 ; \quad N_\theta = \partial^2 F / \partial x^2 \quad \text{and} \quad N_{x\theta} = -(1/R) \partial^2 F / \partial x \partial \theta \quad (25)$$

By making use of the stress strain relationships Eq. (23) and introducing F , we can transform the compatibility relation Eq. (21) to yield the following:

$$\nabla_B^4 F = (B_2/R) (1-\nu^2) \partial^2 w / \partial x^2 \quad (26)$$

where ∇_B^4 is a linear operator given by

$$\nabla_B^4 = \frac{\partial^4}{\partial x^4} + \frac{2}{R^2} \frac{1}{B_1} \left[\frac{B_1 B_2}{B_3} (1+\nu) - \frac{\nu}{2} (B_1 + B_2) \right] \frac{\partial^4}{\partial x^2 \partial \theta^2} + \frac{B_2}{B_1 R^4} \frac{\partial^4}{\partial \theta^4} \quad (27)$$

The third of the equilibrium equations, Eqs. (22), is similarly transformed with the help of Eqs. (23) and (25) to yield:

$$\square^4 w + (1/R) \partial^2 F / \partial x^2 + \bar{N}_x \partial^2 w / \partial x^2 = 0 \quad (28)$$

where \square^4 is a linear operator given by

$$\square^4 = \frac{\partial^4}{\partial x^4} + \frac{2}{R^2} \frac{1}{D_1} \left[D_3 (1-\nu) + \frac{\nu}{2} (D_1 + D_2) \right] \frac{\partial^4}{\partial x^2 \partial \theta^2} + \frac{D_2}{D_1 R^4} \frac{\partial^4}{\partial \theta^4} \quad (29)$$

Eliminating F between Eqs. (26) and (28) we arrive at the governing equation for w as follows

$$\nabla_B^4 (\square^4 w + \frac{\bar{N}_x}{D_1} \partial^2 w / \partial x^2) + \frac{B_2}{D_1 R^2} (1-\nu^2) \frac{\partial^4 w}{\partial x^4} = 0 \quad (30)$$

We define an inverse operator ∇_B^{-4} in the manner of Ref. 2 by the following equation:

$$\nabla_B^{-4} (\nabla_B^4 w) = w \quad (31)$$

With the use of Eq. (31) we can modify Eq. (30) to yield the following governing equation for the pure bending case (i. e. $\bar{N}_x = \bar{N}_b \cos \theta$):

$$L(w) \equiv \square^4 w + \frac{\bar{N}_b}{D_1} \cos \theta \frac{\partial^2 w}{\partial x^2} + \frac{B_2}{R^2 D_1} (1-\nu^2) \nabla_B^{-4} \frac{\partial^4 w}{\partial x^4} = 0 \quad (32)$$

Buckling Mode

Since Eq. (32) cannot be solved exactly for the pure bending case, a suitable form must be assumed for w the normal deflection. From elementary considerations of energy we see that an axisymmetric mode is incompatible with the bending problem. Hence, in the choice of a suitable form for w we may profitably be guided by the buckle pattern in the isotropic case. Though our discussion is perfectly general, it is evident that orthotropic cylinder behavior falls into the classes of longitudinally and circumferentially stiffened cylinders. In both cases, at least in the compressive stability problem, it is usually the wavelength along the longitudinal axis that is modified in comparison with the isotropic cylinder case. Hence so far as the circumferential direction is concerned the buckle pattern should be substantially the same as that of an isotropic cylinder.

Utilizing now the same approximate deflection function employed in Section 3 and shown in Figure 3, we write:

$$\begin{aligned} w &= A \sin(x/\lambda_x^*) \cos N\theta \quad \text{for } |\theta| \leq \pi/2N \\ &= 0 \quad \text{for } \theta \text{ elsewhere on circumference} \end{aligned} \quad (33)$$

where N is a fixed number greater than zero.

Bending Solution

By making use of Eq. (33) for w in Eq. (32), we obtain an expression for \bar{N}_b using the well known Galerkin method. We let

$$\int_0^L \int_{-\pi/2N}^{\pi/2N} L(w) \sin(x/\lambda_x^*) \cos N\theta R d\theta dx = 0$$

and obtain as a result

$$\frac{\bar{N}_b}{D_1} = \frac{\pi/2N}{\sin \pi/2N} \left(1 - \frac{1}{4N^2} \right) \left[\frac{1 + 2 \left\{ (1 - \nu) (D_3/D_1) + \nu/2 (1 + D_2/D_1) \right\} \beta^{*2} + (D_2/D_1) \beta^{*4}}{\lambda_x^{*2}} \right. \\ \left. + \frac{B_2}{R^2 D_1} (1 - \nu^2) \frac{\lambda_x^{*2}}{1 + 2 \left\{ (1 + \nu) (B_2/B_3) - \nu/2 (1 + B_2/B_1) \right\} \beta^{*2} + (B_2/B_1) \beta^{*4}} \right] \quad (34)$$

where: $\beta^* = N\lambda^*/R$

In Eq. (34) the factor $S(N) = \left[(\pi/2N) / \sin(\pi/2N) \right] (1 - 1/4N^2)$ is a function of N only. Furthermore, it is seen to approach unity quite rapidly as N increases in value. In fact even for $N = 2$, S is seen to equal 1.04. Hence for the present problem we assume that N is large enough for $S \approx 1$ and we can write Eq. (34) as

$$\frac{\bar{N}_b}{D_1} \approx \frac{1 + 2 \left[(1 - \nu) D_3/D_1 + \nu/2 (D_1 + D_2)/D_1 \right] \beta^{*2} + (D_2/D_1) \beta^{*4}}{\lambda_x^{*2}} \\ + \frac{B_2}{R^2 D_1} (1 - \nu^2) \frac{\lambda_x^{*2}}{1 + 2 \left[(1 + \nu) B_2/B_3 - \nu/2 (B_1 + B_2)/B_1 \right] \beta^{*2} + (B_2/B_1) \beta^{*4}} \quad (35)$$

Eq. (35) may be recast into the following form which is advantageous in the ensuing discussion:

$$k_b = m^2 [1 + 2\gamma (\overline{\beta^{*2}}/\delta) + \alpha (\overline{\beta^{*4}}/\delta)] + 12(1 - \nu^2) Z^2/\pi^4 [1 + 2\overline{\beta^{*2}}/\delta + \overline{\beta^{*4}}/\delta]^{-1} (1/m^2) \quad (36)$$

where $\gamma = [(1 - \nu) D_3/D_1 + \nu/2 (D_2 + D_1)/D_1] [(1 + \nu) B_2/B_3 - (\nu/2) (B_1 + B_2)/B_1]^{-1}$

$$\alpha = (B_1 D_2)/(B_2 D_1)$$

$$\delta = (B_2/B_1 s^2) \text{ with } s = [(1 + \nu) B_2/B_3 - (\nu/2) (B_1 + B_2)/B_1]$$

$$\overline{\beta^{*2}} = (B_2/B_1 s) \beta^{*2}$$

$$k_b = N_b L^2/\pi^2 D_1 \text{ and } 12Z^2 = B_2 L^4/R^2 D_1$$

It is clear from Eq. (36) that k_b the buckling coefficient is a function of two variables m^2 and $\overline{\beta^{*2}}$. Of these two, $\overline{\beta^{*2}}$ being essentially a function of (L/R) is a continuous variable. However, m^2 or m , which is a measure of the number of buckles along the axis of the cylinder, may take a discrete fixed value or become so large that it can be treated as a continuous variable. In particular $m = 1$ is the lowest discrete value for m , and hence acts as a bound. Thus we may divide the basic asymmetric mode of the bending problem into a $m = 1$ solution and a m - continuous solution.

m - continuous Solution:

Here we consider that k_b in Eq. (36) is a function of m^2 and $\overline{\beta^{*2}}$. The simultaneous vanishing of the first derivatives of k_b with respect to each of m^2 and $\overline{\beta^{*2}}$ being a necessary condition for the minimization of k_b , we set $\partial k_b/\partial m^2 = 0$ and $\partial k_b/\partial \overline{\beta^{*2}} = 0$ from Eq. (36) and obtain as a result the following pair of equations:

$$12(1 - \nu^2) Z^2/\pi^4 (1/m^4) = [1 + 2\gamma \overline{\beta^{*2}}/\delta + \alpha \overline{\beta^{*4}}/\delta] [1 + 2\overline{\beta^{*2}}/\delta + \overline{\beta^{*4}}/\delta] \quad (37)$$

$$12(1 - \nu^2) Z^2/\pi^4 (1/m^4) = [1 + 2\overline{\beta^{*2}}/\delta + \overline{\beta^{*4}}/\delta]^2 (\gamma + \alpha \overline{\beta^{*2}})/(1 + \overline{\beta^{*2}}) \quad (38)$$

Solving Eqs. (37) and (38) we obtain the following expression for $\overline{\beta^{*2}}$

$$\overline{\beta^{*2}} = \delta/2(\alpha - \gamma) [(1 - \alpha) \pm \{(1 - \alpha)^2 + (4/\delta)(1 - \gamma)(\alpha - \gamma)\}^{1/2}] \quad (39)$$

By making use of Eqs. (37) and (38) we obtain finally the following expression for the buckling coefficient k_b :

$$k_b = .702 (1 - \nu^2)^{1/2} Z U^* \quad (40)$$

where $U^* = (\gamma + \alpha \overline{\beta^{*2}})/(1 + \overline{\beta^{*2}})^{1/2} \quad (41)$

In Eqs. (36) through (39) it is possible to obtain further simplification if δ is taken as equal to 1. Since δ is always positive no loss of generality results due to this assumption. Hence in what follows δ is taken as equal to 1.

From Eq. (39) it is clear that $\bar{\beta}^*$ depends upon γ and α (with $\delta = 1$) and for certain γ, α combinations, the quadratic equation yields imaginary values for $\bar{\beta}^*$. It is clear that for these combinations where $\bar{\beta}^*$ is imaginary we have to look for a different solution.

We notice that in Eq. (39) that the lines $\gamma = 1$ and $\gamma = \alpha$ are critical bounds; thus when $\gamma \rightarrow 1$ $\bar{\beta}^* \rightarrow 0$. However, from a fundamental consideration of the bending problem $\bar{\beta}^* = 0$ is to be excluded. Furthermore, we have seen that the reduction of Eq. (34) to Eq. (35) is possible when N is a finite number, but not necessarily very large. Since $\bar{\beta}^*$ is directly dependent on N , we imply by $\bar{\beta}^* \rightarrow 0$ that N is decreasing in value. However, it is clear that when N reaches a certain critical value N^* which is still large enough to admit Eq. (35), the value of $\bar{\beta}^*$ is so small that it has no effect on the problem. Hence when $N = N^*$ as $\gamma \rightarrow 1$ we can neglect terms involving the $\bar{\beta}^{*2}$ and $\bar{\beta}^{*4}$ factors.

Thus we may write a limiting solution for k_b from Eq. (36) as:

$$k_b = m^2 + 12 (1 - \nu^2) Z^2 / (\pi^4 m^2) \quad (42)$$

Limiting Solution

From Eq. (42) k_b is now seen to be a function of m only, for a given cylinder and hence a given Z . Hence if m is large so as to be continuous we obtain from Eq. (42) a minimum value of k_b given by

$$k_b = 2 (12)^{1/2} / \pi^2 Z (1 - \nu^2)^{1/2} = .702 Z (1 - \nu^2)^{1/2} \quad (43)$$

However, since m takes integer values, the lowest value of m is unity. Hence we find:

$$k_{b \ m=1} = 1 + 12 (1 - \nu^2) Z^2 / \pi^4 \quad (44)$$

Now it can be shown quite generally from Eq. (42), that by giving successively higher integer values for m ($m = 2, 3, \text{etc.}$) the curves that are generated have all an envelope which is given by Eq. (43). Furthermore, from the positive nature of the $k - Z$ diagram, this envelope Eq. (43) is a lower bound. Hence a complete minimal curve, which gives the limiting solution, consists of Eq. (44) for low Z values up to the Z value where Eqs. (43) and (44) coincide, and beyond which the

minimal line follows Eq. (43). The value of Z for the contact is easily obtained by equating Eqs. (43) and (44) from which we have:

$$Z^* = \pi^2 / [12 (1 - \nu^2)]^{1/2}$$

Hence the limiting solution is correctly written as

$$\left. \begin{aligned} k_b \text{ lim} &= 1 + 12 (1 - \nu^2) Z^2 / \pi^4 & 0 \leq Z \leq Z^* \\ &= .702Z (1 - \nu^2)^{1/2} & Z^* \leq Z \end{aligned} \right\} \quad (45)$$

The value of N corresponding to this limiting solution is $N = N^*$. The solution given by Eq. (45) is seen to be the same as the axisymmetric solution for the corresponding compressive stability problem. Since Eq. (45) is independent of $\bar{\beta}^*$ this limiting solution may be pertinent in the zones where the m-large solution is not valid.

m = 1 Solution:

Now, we turn to the $m = 1$ solution. In Eq. (36) if we set $m = 1$, then k_b is a function of $\bar{\beta}^{*2}$ only. By setting $\partial k_b / \partial \bar{\beta}^{*2} = 0$ with $m = 1$, we obtain the same expression as Eq. (38) with m replaced by 1. If further we let $\delta = 1$, then we can write from Eq. (38) the following stationary condition for k_b .

$$12 (1 - \nu^2) Z^2 / \pi^4 = (1 + \bar{\beta}^{*2}) (\gamma + \alpha \bar{\beta}^{*2}) \quad (46)$$

Substituting Eq. (44) into Eq. (36), with $m = 1$ and $\delta = 1$, we obtain:

$$k_b \text{ m=1} = 2\alpha \bar{\beta}^{*4} + (3\gamma + \alpha) \bar{\beta}^{*2} + (1 + \gamma) \quad (47)$$

From Eq. (46) it becomes clear that Z increases monotonically with $\bar{\beta}^{*2}$ since γ, α are positive numbers. Furthermore, since Z is always greater than Z_0 corresponding to $\bar{\beta}^* = 0$ in order that an asymmetric mode exist, it is evident that there is always a real positive root for $\bar{\beta}^{*2}$ (and hence real $\bar{\beta}$) for all γ, α values. Hence the $\bar{\beta}^*$ for $m=1$ solution is everywhere real in the γ, α plane.

Comparison of Solutions:

With the three solutions of Eqs. (40), (45) and (47) corresponding to the m-continuous, limiting, and $m=1$ modes respectively, it is pertinent to consider which of these apply in a γ - α plane as in Fig. 4 where the zones are marked from I to VI. We know clearly from Eq. (39) that in zones II and V m-continuous solution does not hold. In other zones all the three are possible. We examine each of the zones more closely.

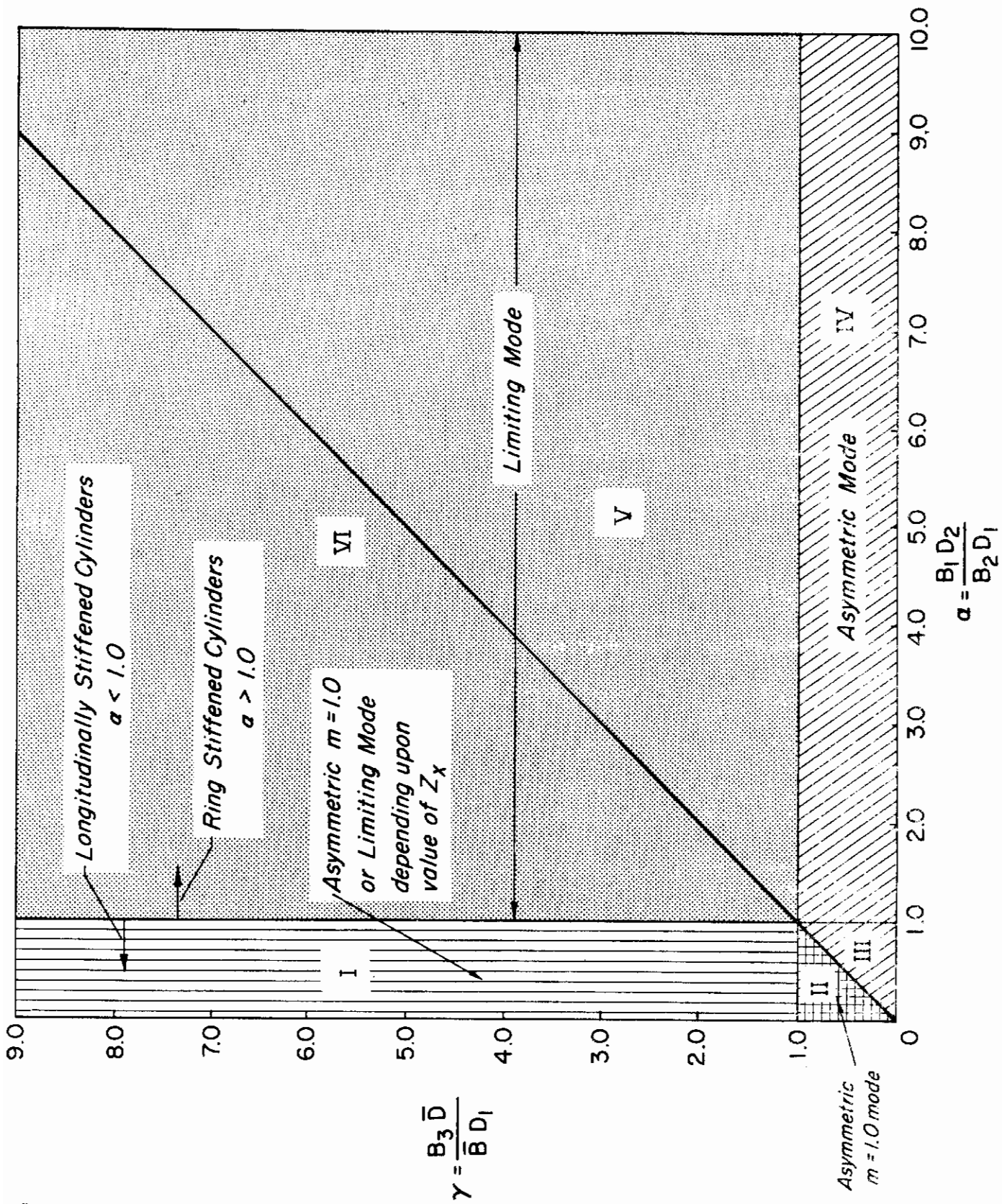


Fig. 4 Characteristics Buckling Domains for Orthotropic Cylinders in Bending.

As regards the $m = 1$ solution we have seen that it applies in every zone of γ - α plane and so too does the limiting solution. The behavior of $m = 1$ solution in all the zones is easily predicted since we need only consider the limiting values of $\bar{\beta}^{*2}$. In comparing the $m = 1$ solution with the limiting solution, we first observe that in view of Eqs. (45) and (46), the buckling coefficient for the limiting solution may be written as:

$$k_{b \text{ lim}} = 2 [(\gamma + \alpha \bar{\beta}^{*2}) (1 + \bar{\beta}^{*2})^3]^{1/2}$$

then

$$\frac{k_{b \text{ m=1}}}{k_{b \text{ lim}}} = \frac{2\alpha \bar{\beta}^{*4} + (3\gamma + \alpha) \bar{\beta}^{*2} + (1 + \gamma)}{2 [(\gamma + \alpha \bar{\beta}^{*2}) (1 + \bar{\beta}^{*2})^3]^{1/2}} \quad (48)$$

we find that for low $\bar{\beta}^{*2}$ values, (i. e. low Z values):

$$\bar{U}^* = \frac{k_{b \text{ m=1}}}{k_{b \text{ lim}}} = (1 + \gamma) / 2\gamma^{1/2} \quad (49)$$

and for large $\bar{\beta}^{*2}$ values, (i. e. large Z values):

$$\bar{U}^* = \frac{k_{b \text{ m=1}}}{k_{b \text{ lim}}} = \alpha^{1/2} \quad (50)$$

Eqs. (49) and (50) together with Eq. (41) then summarizes the comparison of different solutions in the different zones.

In zones II and V only the limiting solution and the $m=1$ solution are possible while every where else all the three solutions are possible. However, to find which one is the lowest and hence the correct buckling solution we shall examine each zone in detail.

In zones V and VI, both γ and α are ≥ 1 . Hence Eqs. (49) and (50) show that $k_{b \text{ m=1}} / k_{b \text{ lim}} \geq 1$ for all Z ranges. Hence $k_{b \text{ lim}}$ is the lowest bound solution in the interior in comparison with $m=1$ solution. As regards m -continuous solution, it comes in only in zone VI. But in this zone, with $\gamma \geq \alpha$, $(\gamma, \alpha) \geq 1$ it can be shown that U^* of Eq. (41) is always an upper bound over the \bar{U}^* value. Hence in zone VI $k_{b \text{ m=1}} \geq k_{b \text{ lim}}$. As for the lines $\gamma = 1$ and $\alpha = 1$ in this zone, the asymptotic behavior is warranted by Eqs. (49) and (50). Thus along the $\gamma = 1$ line Eq. (49)

shows that for low Z values m=1 solution and k_{lim} solutions coincide but with $\alpha = 1$, as Z increases $k_{m=1}$ becomes greater than k_{lim} . The actual shape and the point of separation is dependent on the value of α . Similarly on the line $\alpha = 1$, $k_{m=1}$ solution approaches the k_{lim} solution from above for high values of Z and actual shape depends upon Z the γ value chosen.

In zone I $\gamma \geq 1$ but $\alpha \leq 1$. Hence from Eq. (50) we see that for higher values of Z, $k_{m=1}$ becomes less than k_{lim} solution. While in this entire zone $k_{m-cont.}$ is always an upper bound and is always greater than k_{lim} solution, zone I behavior may be summarized as:

$$k_{b \ m-cont.} > k_{b \ lim}; \quad k_{b \ m-cont.} \geq k_{b \ m=1} \geq k_{b \ lim}$$

In zone II both γ and α are ≤ 1 . In the interior of this region only $k_{m=1}$ and $k_{b \ lim}$ solutions are real; further, since both γ and $\alpha < 1$, Eqs. (49) and (50) show that $k_{b \ m=1} < k_{b \ lim}$. On the line $\gamma = \alpha$, it turns out that both $k_{b \ m=1}$ and $k_{b \ m-cont.}$ are possible: Eq. (39) shows that $\bar{\beta}^{*2}$ for m-cont case $\rightarrow \infty$ on this line. Then Eq. (41) shows that along the line $U^+ = \alpha^{1/2}$. But this is precisely true for $k_{m=1}$ solution also for large values of Z as seen in Eq. (50). Hence $k_{m=1}$ solution merges with $k_{m-cont.}$ solution for higher values of Z.

In zones III and IV, the m-cont. solution is real, and also forms the lower envelope of the m-discrete solutions and hence is the lower bound. $k_{b \ m-cont.}$ may be considered as prevailing from the value of Z where the m=1 solution touches it. That is, the m=1 solution is the correct solution for low values of Z and beyond the Z value where the two solutions coincide, the $k_{m-cont.}$ solution is the correct one. While m=1 solution becomes greater than m-cont. solution for higher Z values, yet it will be lower than k_{lim} value so long as $\alpha < 1$ (i. e. in zone III), but in zone IV with $\alpha > 1$ the m=1 solution will eventually exceed k_{lim} solution. Thus for zone III:

$$k_{b \ lim} \geq k_{b \ m=1} \geq k_{b \ m-cont}$$

for zone IV:

$$k_{b \ lim} > k_{m-cont}; \quad k_{b \ lim} < k_{m=1}; \quad k_{b \ m=1} \geq k_{b \ m-cont.}$$

Compressive Stability:

In order to compare the bending stability of an orthotropic cylinder with that of the compressive stability, we abstract some of the chief results from Ref. 1 and Ref. 3 which deal with the latter case.

As a pure axisymmetric mode is possible in the compressive stability case, so the w function is chosen as $w = A \sin \frac{m\pi x}{L} \cos n \theta$; $n \geq 0$. (51)

Defining $\beta = nL/m\pi R$, where m is as before the number of axial buckles, we obtain for the compressive case, following solutions for the compressive buckling coefficient k_c :

Axisymmetric Solution ($\beta = 0$)

$$\left. \begin{aligned} k_c &= 1 + 12(1 - \nu^2) Z^2/\pi^4 & 0 \leq Z \leq Z^* \\ &= .702 Z (1 - \nu^2)^{1/2} & Z^* \leq Z \end{aligned} \right\} \quad (52)$$

where

$$Z^* = \pi^2/[12(1 - \nu^2)]^{1/2}$$

Asymmetric Solution ($\beta > 0$)

$$k_{c \text{ m-cont.}} = .702 Z (1 - \nu^2)^{1/2} U \quad (53)$$

where

$$U = [(\gamma + \alpha\bar{\beta}^2)/(1 + \bar{\beta}^2)]^{1/2} \quad \text{and} \quad \bar{\beta}^2 = [B_2/B_{1s}]\beta^2$$

and $\bar{\beta}^2$ satisfies an equation identical with Eq. (39), namely:

$$\bar{\beta}^2 = \delta/2 (\alpha - \gamma) \left[(1 - \alpha) \pm \left\{ (1 - \alpha)^2 + 4/\delta (1 - \alpha) (\alpha - \gamma) \right\}^{1/2} \right] \quad (54)$$

$$k_{c \text{ m=1}} = 2\alpha\bar{\beta}^4 + (3\gamma + \alpha)\bar{\beta}^2 + (1 + \gamma) \quad (55)$$

where δ is taken as 1.

In Eqs. (54) and (55) γ , and α are the same as defined in Eq. (36).

Ref. 1 discusses the various zones of γ - α plane where the solution of Eqs. (52) to (55) apply and their significance.

Comparison of Bending and Compressive Stability:

An examination of Eqs. (52) to (55) show that they are identical with the similar expressions for the buckling coefficient k_b in Eqs. (40), (41), (45) and (47). Further, the quadratic equation for $\bar{\beta}^*$ (Eq. 39) is identical to that for $\bar{\beta}$ in Eq. 54. Hence, it is clear that $\bar{\beta}^*$ and $\bar{\beta}$ are equal whenever the solutions are applicable. While in Eq. (54) $\bar{\beta}$ can actually attain limiting value of zero for $\gamma = 1$ ($n=0$), $\bar{\beta}^2$ cannot do so. However, when $N \rightarrow N^*$, the limiting solution of Eq. (45) which is equivalent to the axisymmetric solution of k_c Eq. (52) applies.

Hence it follows that while in the compressive case the buckling mode changes from a general asymmetric pattern to an axisymmetric one as $\beta \rightarrow 0$, the behavior in the bending case is different. To start with, we have a single lobe whose half width is given by $\pi/2N$; and the displacement is zero everywhere else. As N becomes large the influence of β^* is great; while as N becomes small it reaches a limiting value $N = N^*$ (and the mode, correspondingly, a limiting mode), when the influence of β^* is negligible.

Regarding the stress picture from the identity of the sets of equations for k_c and k_b , it follows that k_b and k_c have identical behavior in all the zones of a γ - α plane as in Fig. 4. Hence, summarizing we find that $k_b/k_c = 1$ in the entire γ - α plane.

Concluding Remarks

The behavior in the bending stability problem is generally governed by the fact that the external stress distribution changes from a compressive one at the top to a tensile one at the bottom half of a cross section of the cylinder. This precludes any buckling effect on the tension side. Hence a compatible buckle pattern for the bending problem has to be deflection free on the tension side. Hence, a general type of asymmetric mode with ripples running all the way around the circumference, which is perfectly suitable in a compressive stability problem, becomes impossible in the bending case. A suitable pattern seems to have a single lobe symmetric about a vertical axis and whose maximum width is a small fraction of π which is signified by π/N , where N is usually a large number. Thus the buckling pattern presents a widely differing picture in the bending case as compared to the compressive case.

However, when we turn to the stress picture we find that for both the isotropic cylinders and for the orthotropic cylinders k_b/k_c is essentially equal to unity.

SECTION 5 BENDING TESTS

Design and Fabrication of Test Specimens

Bending tests were performed on ring stiffened, longitudinally stiffened, and grid stiffened cylinders. The cylinder geometries encompassed an α range from 0.1 to 12.0. All specimens were designed to fail in the general instability mode at a stress level below the proportional limit of the material.

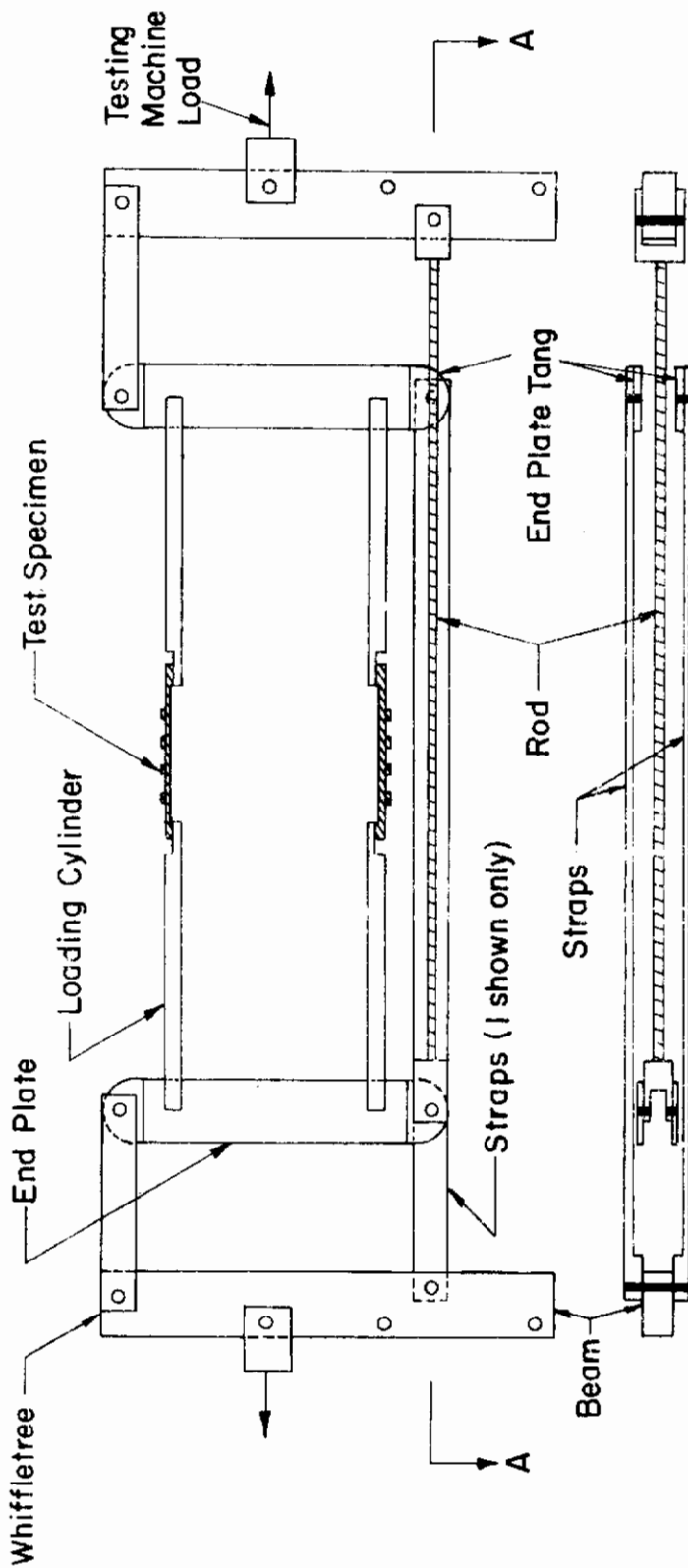
The detailed design technique for bending test specimens characterized by $\alpha > 1.0$ was the same as that used for ring stiffened axial compression test specimens and is described in Ref. 1. In general, the design procedure includes the selection of cross sectional proportions to achieve the desired α value together with a cylinder radius/wall thickness ratio as dictated by the design buckling stress. Finally, a suitable value for the cylinder length/radius ratio was chosen to achieve moderate-length cylinder behavior. Typical design curves for axial compression specimens which are also applicable for bending specimen design are presented in Sec. 4 of Ref. 1.

For longitudinally stiffened bending specimens ($\alpha < 1.0$), the cylinder cross-sectional proportions followed from design α requirements as above. In this case, selection of a design value of the radius/wall thickness ratio was facilitated through use of an approximate relationship for the critical buckling stress. As observed in Sec. 2 of Ref. 1, the buckling stress for cylinders which fail in the asymmetric $m = 1$ buckling mode is approximately equal to the classical theoretical buckling stress for an isotropic cylinder with the same radius/thickness ratio. This relationship was used for the $\alpha < 1.0$ specimen design. Reduction of test data, however, was based on a rigorous asymmetric theory as described below.

Test specimens were machined on a lathe from an aluminum 6061-T6 tube. Longerons and frame stiffening elements were integrally formed in the cylinder wall. Reinforcing rings were fabricated at the cylinder ends to facilitate adaption of the test specimen to the test fixture. A detailed discussion of the fabrication technique is presented in Sec. 4 of Ref. 1.

Test Arrangement and Procedure

A schematic of the test fixture for performing bending tests on the test specimens is shown in Fig. 5. One can deduce from the figure that the testing machine axial load is transformed to a couple loading on the end plates by means of the whiffletree linkage arrangement. The couple load is then diffused as a distributed bending moment through the loading cylinder to the test specimen. By



Sec. A-A

Fig. 5 Schematic of Bending and Combined Loading Test Fixture.

applying the testing machine load at various positions along the whiffletree beam combinations of bending load and axial compressive loading are achieved.

Fig. 6 shows the test arrangement including pre-test and post failure photographs of a grid stiffened cylinder (Specimen No. 60). One observes that the specimen was attached to the loading cylinder via closely spaced dowel pins. Post failure rotations of the specimen were limited by a stop arrangement on the test machine. Photographs of representative cylinder configurations failed via bending loading are presented in Fig. 7.

Accuracy of Experimental Data

Experimental data necessary to evaluate the test results include maximum cylinder bending moment and the specimen geometric parameters, length, radius, wall thickness, total height, stiffener width, and stiffener spacing. Values for the critical specimen bending moment followed from the test machine pressure loading at cylinder failure together with test fixture linkage geometry. Failure of all but one of the test specimens occurred at test machine pressures from 39 to 56 psi. Since the gage of the test machine could be read to a precision of 0.25 psi and the test fixture geometry was accurately measured within 1%, the indicated accuracy of the bending moment corresponding to specimen failure was within 1.6%. One test specimen (RSC No. 63) failed at a test machine pressure loading of 7.5 psi for which the indicated accuracy of the bending moment at failure was within 3.4%.

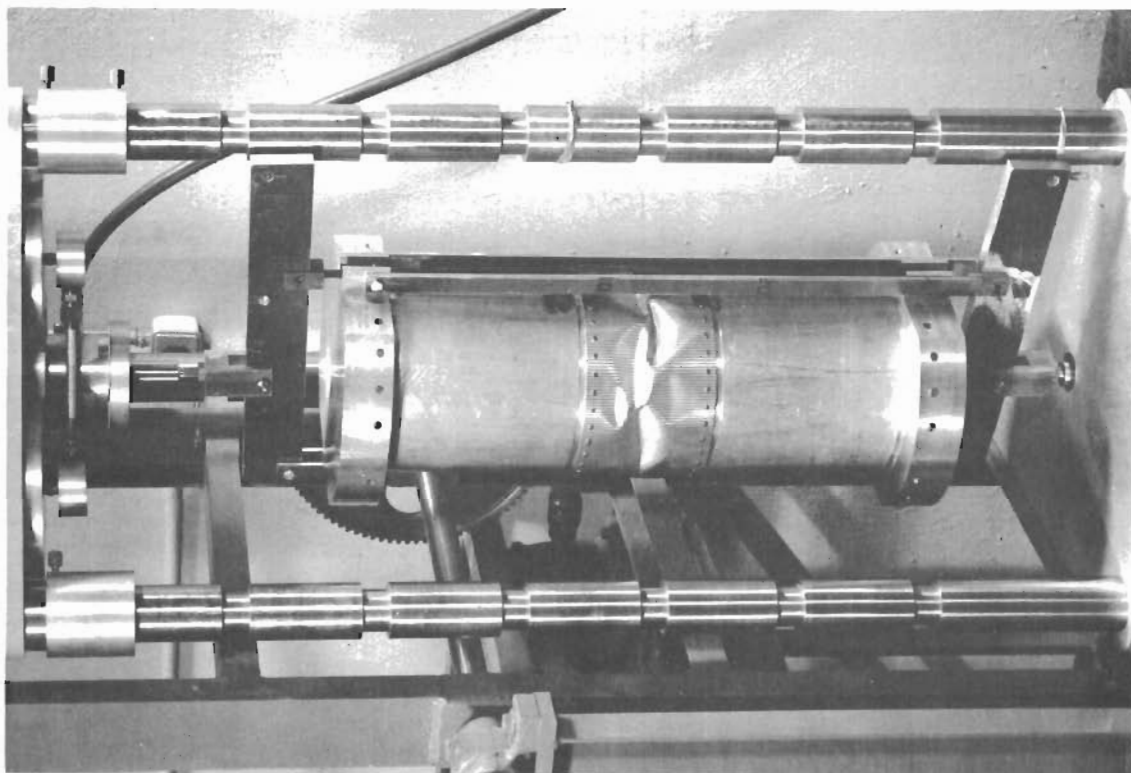
Experimental data associated with cylinder geometry are tabulated below (see Table 1) together with estimates of the measurement error and the corresponding percent measurement error. As indicated by the table, the maximum measurement error was 5.4% and was associated with measurements of the cylinder wall thickness.

Table 1

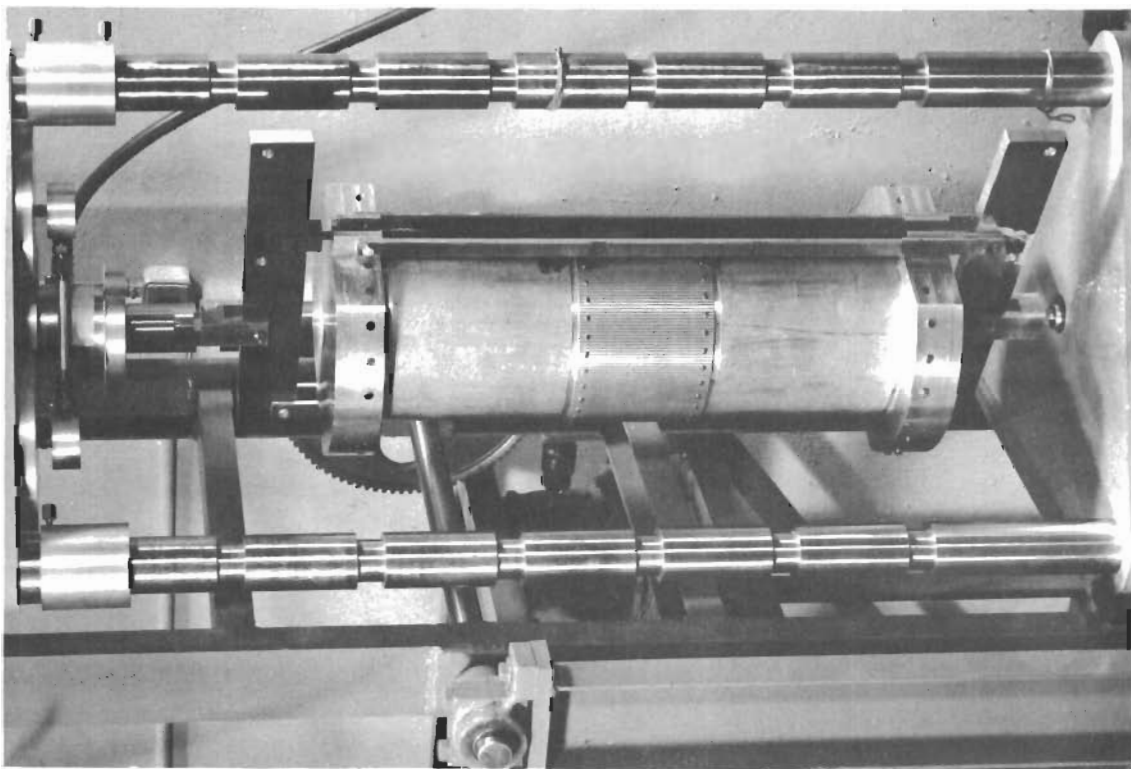
Accuracy of Experimental Data for Bending Specimens

Parameter	L	R	w	d	t	h
Minimum Value (in.)	1.80	3.80	.049	.111	3.7×10^{-3}	13.9×10^{-3}
Average Value (in.)	3.15	3.80	.055	.115	9.5×10^{-3}	17.1×10^{-3}
Maximum Value (in.)	3.82	3.80	.061	.120	12.5×10^{-3}	23.9×10^{-3}
Measurement Error (10^{-3} in.)	.5	.5	2.0	2.0	.2	.2
% Error (1)	.02	.01	4.0	1.8	5.4	1.4
% Error (2)	.02	.01	3.6	1.7	2.1	1.2
% Error (3)	.01	.01	3.3	1.7	1.6	.8

(1) Based on Minimum values (2) Based on Average values (3) Based on Maximum values

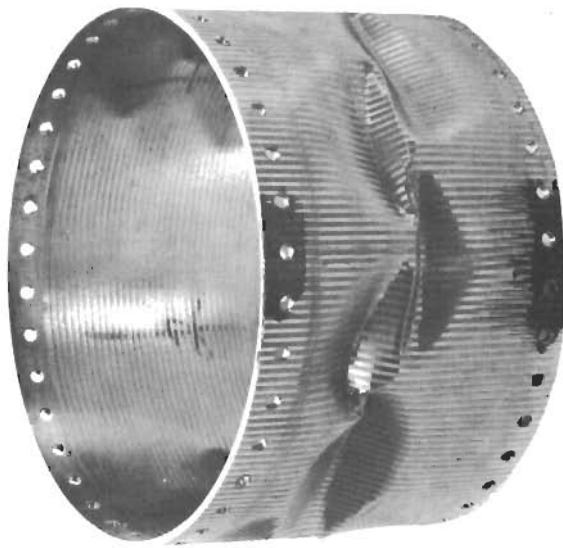


Post Failure
(Specimen No. 60)

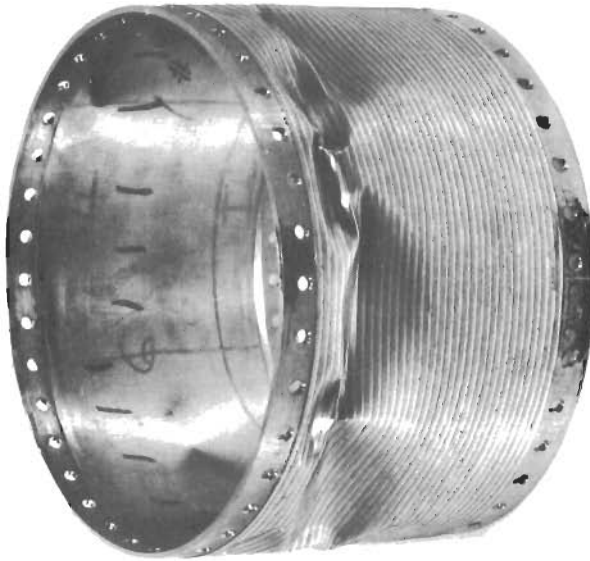


Pre-Test
(Specimen No. 60)

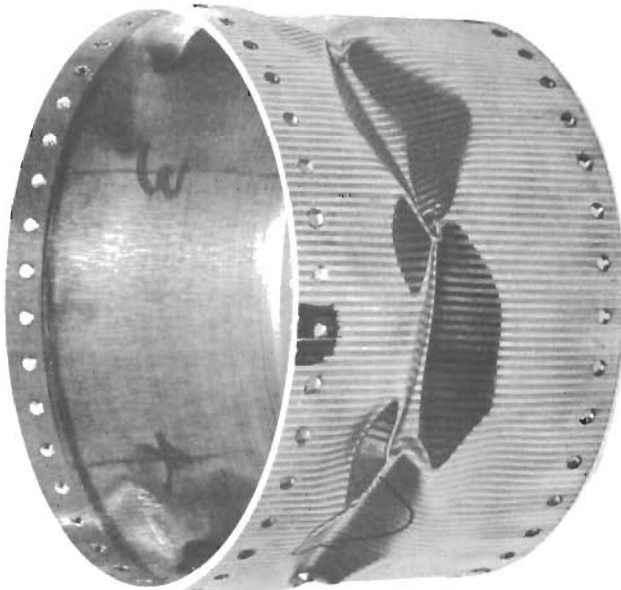
Figure 6. Photographs of Specimen No. 60 Buckled by Bending Load.



Grid Stiffened Cylinder
(Specimen No. 60)



Ring Stiffened Cylinder
(Specimen No. 62)



Longitudinally Stiffened Cylinder
(Specimen No. 65)

Figure 7. Post Failure Bending Specimens.

Reduction of Test Data on Failure of Cylinders

Evaluation of test results required data for the experimental bending moment, maximum stress, and buckling coefficient. The critical bending moment was obtained by multiplying the test fixture couple arm (9.0 in.) by the couple load as determined by the test machine pressure load at specimen failure, the machine calibration factor, and the test fixture linkage geometry. For bending tests the test apparatus was arranged such that one half the total axial load on the test machine was distributed to each linkage (see Fig. 5). Hence,

$$M_{\text{exp}} = (p_{\text{exp}} \times C/2) 9.00 \quad (56)$$

The maximum cylinder bending stress at failure was determined by dividing the bending moment by the cylinder section modulus.

$$\sigma_{\text{b exp}} = M_{\text{exp}} / (\pi t_s R^2) \quad (57)$$

Since the critical stress in bending and axial compression are theoretically equal, values for the experimental buckling coefficient in bending were determined by dividing the failure stress by the same cylinder material and geometry used for the determination of the axial compression experimental buckling coefficient (Ref. 1). Thus,

$$k_{\text{b exp}} = \sigma_{\text{b exp}} / F_x \quad (58)$$

where $F_x = \pi^2 E I_s / t_s L^2 \quad (59)$

Substitution of Eq. (59) in (58) gives

$$k_{\text{b exp}} = \sigma_{\text{b exp}} [t_s L^2 / (\pi^2 E I_s)] \quad (60)$$

It is noted that Eqs. (59) and (60) are based on the assumption that Poisson's ratio is zero.

The parameters (t_s , I_s) appearing in the above equations together with other geometrical and rigidity parameters presented below were calculated using methods presented in Sec. 3 of Ref. 1 and were based on average values for cylinder measurements. All data were reduced based on $E = 10.1 \times 10^6$ psi which corresponds to an aluminum 6061-T6 material. As noted previously Poisson's ratio was assumed equal to zero.

Values for cylinder cross sectional measurements necessary for calculation of geometric parameters were determined as follows: For ring stiffened and longitudinally stiffened cylinders, pre-test measurements of both the cylinder wall thickness and the total height at a stiffener were made at six circumferential locations at each end of the specimens. Thus average values for wall thickness and total height were based on a total of twelve measurements for each parameter. For grid stiffened designs, this procedure resulted in average values based on twelve measurements each for the wall thickness, total height at a frame, and total height at a longeron. It is noted that all test data were reduced based on pre-test measurements only.

A summary of material, geometrical and rigidity parameters for bending test specimens is presented in Table 2 and the experimental structural parameters are summarized in Table 3.

Calculation of Theoretical Structural Parameters

As shown in Sec. 4 the theoretical critical stress for orthotropic cylinders under bending or axial compressive loading are equal. Hence, equations and methods for the determinations of theoretical structural parameters for bending applications are the same as those presented for axial compressive loading in Ref. 1. These equations are recapitulated below for sake of completeness. A more detailed exposition is presented in Sec. 4 and Appendix A of Ref. 1.

The buckling mode for orthotropic cylinders subject to general instability can be characterized by the geometric parameters α , γ , and δ defined as follows (Ref. 1).

$$\begin{aligned}\alpha &= t_s I_f / (t_f I_s) \\ \gamma &= (1/4) (E/t_f) (J/I_s) \\ \delta &= \bar{r}^2 / (t_s t_f)\end{aligned}\tag{61}$$

For bending specimens with $\alpha > 1.0$ (all the ring stiffened and grid stiffened designs), values for the cylinder geometry parameters α and γ (see Table 3) were such that the axisymmetric buckling mode governed ($U = 1.0$). In such cases the curvature parameter, buckling coefficient, and corresponding stress are

given by (Ref. 1)

$$Z_x = (12)^{-1/2} (t_f / I_s)^{1/2} (L^2 / R) \quad (62)$$

$$k_x = .203 (t_f / I_s)^{1/2} (L^2 / R) \quad (63)$$

$$\sigma_x = 2E (t_f I_s)^{1/2} / (Rt_s) \quad (64)$$

Bending specimens with $\alpha < 1.0$ (all longitudinally stiffened cylinders) are subject to buckling in the asymmetric $m = 1$ mode. From Ref. 1 the curvature and buckling coefficient are determined from the following equations

$$Z_x = [1 + 2 (\bar{\beta}^2 / \delta) + (\bar{\beta}^4 / \delta)]^2 (\gamma + \alpha \bar{\beta}^2) [(1 + \bar{\beta}^2) 12 / \pi^4]^{-1} \quad (65)$$

$$k_x = 1 + 2\gamma (\bar{\beta}^2 / \delta) + \alpha (\bar{\beta}^4 / \delta) + [1 + 2 (\bar{\beta}^2 / \delta) + (\bar{\beta}^4 / \delta)] (\gamma + \alpha \bar{\beta}^2) (1 + \bar{\beta}^2) \quad (66)$$

For a given specimen geometry and assumed values of $\bar{\beta}$, a curve of k_x vs. Z_x was constructed through use of Eqs. (65) and (66). The theoretical value for the buckling coefficient was then determined from the curve for the design value of Z_x .

Once the theoretical buckling coefficient was known the corresponding theoretical buckling stress was calculated using the following general relationship (Ref. 1).

$$\sigma_x = k_x (\pi^2 E I_s / t_s L^2) \quad (67)$$

It is noted that all equations presented above are based on the assumption that $\nu = 0$.

The theoretical bending moment in all cases was determined from the product of the buckling stress and section modulus as shown

$$M_b = \sigma_x (\pi t_s R^2) \quad (68)$$

A summary of the theoretical parameters for the bending specimens is presented in Table 3.

TABLE 2
Material, Geometrical, and Rigidity Parameters for Bending Test Specimens

Ring Stiffened and Longitudinally Stiffened Cylinders																
Spec. No.	Type	L	R	w	d	t	t/b	b	t _s	t _f	\bar{t}	I _s /b ³	I _f /b ³	J/b ³	E	
Col.	2	3	4	5	6	7	8	9	10	11	12	13	14	15	16	
Ref.	--	--	--	--	--	--	--	--	--	--	**	--	--	--	--	
Units	in.	in.	in.	10 ⁻³ in.	10 ⁻³ in.	10 ⁻³ in.	10 ⁻³ in.	10 ⁻³ in.	10 ⁻³ in.	10 ⁻³ in.	10 ⁻² in ³ /in ³	10 ⁻² in ³ /in ³	10 ⁻² in ³ /in ³	10 ⁻² in ³ /in ³	psi	
62	RSC*	3.83	3.80	51	111	11.3	2.62	4.3	11.3	13.3	12.3	150	295	1010	10.1 x 10 ⁶	
63	RSC	2.00	↑	54	111	4.4	.433	10.2	4.4	9.4	6.9	.674	16.5	42	↑	
65	LSC ^φ	3.73	↓	60	120	11.3	2.81	4.0	13.3	11.3	12.3	340	185	1250	↓	
66	LSC	3.77	3.80	59	119	8.1	.509	15.9	15.9	8.1	12.0	19.5	1.1	41.9	10.1 x 10 ⁶	

Grid Stiffened Cylinders																			
Spec. No.	L	R	w _s	d _s	t	t/b _s	b _s	w _f	d _f	t/b _f	b _f	t _s	t _f	\bar{t}	I _s /b _s ³	I _f /b _f ³	J/b _s ³	E	
Col.	2	3	4	5	6	7	8	9	10	11	12	13	14	15	16	17	18	19	
Ref.	--	--	--	--	--	--	--	--	--	**	--	--	--	--	--	--	--	--	--
Units	in.	in.	10 ⁻³ in.	10 ⁻³ in.	10 ⁻³ in.	10 ⁻³ in.	10 ⁻³ in.	10 ⁻³ in.	10 ⁻³ in.	10 ⁻³ in.	10 ⁻³ in.	10 ⁻³ in.	10 ⁻³ in.	10 ⁻³ in.	10 ⁻² in ³ /in ³	10 ⁻² in ³ /in ³	10 ⁻² in ³ /in ³	psi	
60	3.81	3.80	57	119	11.4	2.56	4.5	50	111	2.25	5.1	13.5	13.7	13.6	275	200	1630	10.1 x 10 ⁶	
64	1.80	3.80	59	119	10.3	1.88	5.5	49	111	.94	11.0	13.0	15.3	14.1	137	39.3	1575	10.1 x 10 ⁶	

** See Table 3.2 Ref. 1

* RSC = Ring Stiffened Cylinder

φ LSC = Longitudinally Stiffened Cylinder

TABLE 3
Bending Loading - Summary of Structural Parameters

Spec. No.	Type	α	γ	δ	$M_{exp.}$	M_b	$\sigma_{b, exp.}$	σ_x	$k_{b, exp.}$	k_x	Z_x
Col.		3	4	5	6	7	8	9	10	11	12
Ref.	--	$\overline{\gamma}$	$\overline{\gamma}$	\rightarrow	Eq. (56)	Eq. (68)	Eq. (57)	Φ	Eq. (58)	ϕ	Δ
Units	--	--	--	--	$\rightarrow 10^3$ in. lbs.	$\rightarrow 10^3$ psi	\rightarrow	\rightarrow	--	--	--
62	RSC*	1.68	1.56	--	9.31	9.54	18.2	18.7	250	256	365
63	RSC	11.6	11.4	--	1.79	1.94	9.0	9.75	225	244	348
65	LSC**	.64	1.0	1.0	9.44	10.1	15.6	16.7	131	140	239
66	LSC	.11	.80	1.12	10.0	10.2	13.9	14.2	40.7	41.5	110
60	GSC***	1.06	1.48	--	13.4	13.8	21.9	22.6	178	184	262
64	GSC	1.98	2.66	--	12.1	13.9	20.6	23.6	39	45	64.2

Φ Eq. (64) for RSC and GSC, Eq. (67) for LSC
 ϕ Eq. (63) for RSC and GSC, See Text for LSC
 Δ Eq. (62) for RSC and GSC, See Text for LSC
 * RSC = Ring Stiffened Cylinder
 ** LSC = Longitudinally Stiffened Cylinder
 *** GSC = Grid Stiffened Cylinder
 $\overline{\gamma}$ See Eq. (4.8) of Ref. 1

SECTION 6
COMBINED LOADING TESTS

Design and Fabrication of Test Specimens

Combined loading (axial compression plus bending loading) tests were performed on a ring stiffened and longitudinally stiffened cylinder with design α values of 1.6 and 0.1, respectively. Both specimens were designed to fail in the general instability mode at a maximum combined stress level below the proportional limit of the material. The design technique was the same as outlined in Sec. 5 for the bending specimens. As before, the specimens were machined from an aluminum 6061-T6 tube. The stiffening elements were integrally formed in the cylinder wall and heavy rings were fabricated at the cylinder ends to facilitate mounting the specimens on the test fixture. See Ref. 1 for a detailed discussion of the specimen fabrication process.

Test Arrangement and Procedure

The test arrangement and procedure for the combined loading tests were the same as that for the bending tests. As indicated in Sec. 5, the test fixture was designed such that either pure bending or combined bending and compression loads could be applied to the test specimen. For the combined loading condition, the test machine axial load was applied at the whiffletree beam holes offset from the centroid of the cylinder longitudinal axis (see Figs. 5 and 6).

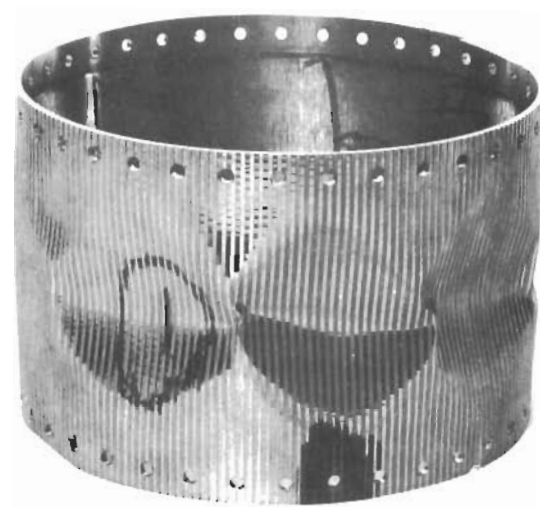
Post failure photographs of the two specimens failed under combined loading are presented in Fig. 8.

Accuracy of Experimental Data

Test machine pressure loading for the ring stiffened and longitudinally stiffened cylinders were 21 and 23.8 psi, respectively. This pressure could be read to a precision of 0.25 psi and the indicated accuracy of the total load applied to the test specimens is within 1.2%. Other experimental data in the form of geometrical parameters are tabulated below together with the estimated measurement error (see Sec. 4 - Ref. 1) and % error. One observes that the maximum % error is associated with measurements of the stiffener width and has a value of 4%



Ring Stiffened Cylinder
(Specimen No. 67)



Longitudinally Stiffened Cylinder
(Specimen No. 68)

Figure 8. Failure Combined Loading Specimens.

Table 4

Accuracy of Experimental Data for Combined Loading Tests

Parameter	L	R	w	d	t	h
Minimum Value (in.)	3.68	3.80	50	111	7.2	15.1
Average Value (in.)	3.72	3.80	55	115	9.8	19.9
Maximum Value (in.)	3.75	3.80	59	119	13.0	24.6
Measurement Error (10^{-3} in.)	.5	.5	2.0	2.0	.2	.2
%Error (1)	1.4	1.3	4.0	1.8	2.8	1.3
%Error (2)	1.3	1.3	3.6	1.7	2.0	1.0
%Error (3)	1.3	1.3	3.4	1.7	1.5	.8

(1) Based on Minimum value (2) Based on Average value (3) Based on Maximum value

Reduction of Test Data on Failure of Cylinders

The distribution of the total axial load applied by the testing machine to the test fixture into components of axial compressive force and bending moment in the test specimen was controlled by the geometry of the point of application of the applied load and its reactions on the whiffletree beam (see Fig. 5). A test arrangement was chosen wherein the distribution of load was such that the specimens were loaded to approximately 50% of their ultimate strength in both axial compression and pure bending at failure. Based on the test fixture and specimen geometry, this corresponded to a net axial compressive force and bending moment as follows:

$$P_{\text{exp}} = (p_{\text{exp}} C) 2 \quad (69)$$

$$M_{\text{exp}} = (p_{\text{exp}} C) 4.5 \quad (70)$$

The compressive stress due to the axial load was determined by dividing this load by the specimen cross sectional area.

$$\sigma_{\text{c exp}} = P_{\text{exp}} / (2\pi R t_s) \quad (71)$$

As in Sec. 5, the maximum bending stress was found by dividing the bending moment by the specimen section modulus (Eq. 57).

All geometrical and rigidity parameters in these equations were evaluated using methods presented in Sec. 3 of Ref. 1 and were based on average values for cylinder measurements. The technique for obtaining these measurements was the same as for the bending specimens (see Sec. 5).

A summary of the geometrical and rigidity parameters for the specimens is presented in Table 5. Experimental values for the structural parameters are given in Table 6.

Calculation of Theoretical Structural Parameters

The ring stiffened cylinder geometric parameters α and γ were such that the axisymmetric buckling mode governed and the corresponding critical buckling stress for both axial compression and pure bending was obtained using Eq. (64).

For the longitudinally stiffened specimen, the $m=1$ asymmetric mode governs and the buckling stress was determined through use of Eqs. (65), (66) and (67).

The structural parameters are summarized in Table 6.

Calculation of Stress Ratios

Theoretical considerations presented in Sec. 4 indicate that a linear interaction law holds for predicting the strength of orthotropic cylinders under combined axial compression and bending. Based on stress considerations, this linear interaction relationship has the following form

$$R_c + R_b = 1.0$$

or

(72)

$$\sigma_c / \sigma_x + \sigma_b / \sigma_x = 1.0$$

Evaluation of the above failure law based on experimental results was accomplished as follows: the components of the compressive and bending stress corresponding to specimen failure were calculated based on experimental results using Eqs. (69), (70), (71) and (57). The theoretical critical stress (for both axial compression and bending) was determined as indicated in the section on "Calculation of Theoretical Structural Parameters." Finally, the stress ratios based on axial load and pure bending, R_c and R_b , were calculated by dividing the experimental

Contrails

value of the stress component by the theoretical buckling stress (Eq. 72). Values for the stress ratios based on the above procedure are given in Table 6.

TABLE 5

Material, Geometric and Rigidity Parameters for Combined Loading Test Specimens

Spec. No.	Type	L	R	w	d	t	t/b	b	t _s	t _f	\bar{t}	I _s /b ³	I _f /b ³	J/b ³	E
Col.	2	3	4	5	6	7	8	9	10	11	12	13	14	15	16
Ref.	--	--	--	--	--	--	--	--	--	--	--	--	--	--	--
Units	--	in.	in.	in.	10 ⁻³ in.	in.	--	in.	10 ⁻³ in.	in.	10 ⁻² in ³ /in ³	in ³	in ³	in ³	psi
67	RSC ^φ	3.75	3.80	50	111	11.6	2.65	4.4	11.6	13.5	12.5	150	290	1025	10.1 x 10 ⁶
68	LSC [⊓]	3.68	3.80	59	119	7.9	.50	16.0	15.9	7.9	11.9	19	1.02	40.7	10.1 x 10 ⁶

TABLE 6

Combined Loading - Summary of Structural Parameters

Spec. No.	Type	α	γ	δ	M _{exp.}	P _{exp.}	σ _{b exp.}	σ _{c exp.}	σ _x	R _b	R _c
Col.	2	3	4	5	6	7	8	9	10	11	12
Ref.	--	Eq. (61)	Eq. (61)	Eq. (70)	Eq. (69)	Eq. (57)	Eq. (71)	Eq. (72)	--	Eq. (72)	--
Units	--	--	--	10 ³ in.lbs.	10 ³ lbs.	10 ³ lbs.	10 ³ psi	10 ³ psi	--	--	--
67	RSC ^φ	1.6	1.59	--	5.02	2.22	9.6	8.05	19.4	.50	.42
68	LSC [⊓]	.11	.80	1.13	5.66	2.52	7.89	6.65	13.4	.59	.50

φ RSC - Ring Stiffened Cylinder

⊓ LSC = Longitudinally Stiffened Cylinder

* See Table 3.2 Ref. 1.

** Equation (64) for RSC

See Text for LSC

REFERENCES

1. Milligan, R., Gerard, G., Lakshmikantham, C. and Becker, H., General Instability of Orthotropically Stiffened Cylinders, Part I - Axial Compression, Torsion and Hydrostatic Pressure Loading, AFFDL-TR-65-161, Part I, July 1965.
2. Seide, P. and Weingarten, V. I., "On the Buckling of Circular Cylindrical Shells Under Pure Bending," Jour. Appl. Mech., Vol. 28, Series E. No. 2, 1961.
3. Gerard, G., "Compressive Stability of Orthotropic Cylinders," Jour. Aerospace Sciences, Vol. 29, No. 10, pp. 1171-1180, October 1962.
4. Taylor, J. L., "The Stability of a Monocoque in Compression," British R and M No. 1679, June 1935.
5. Becker, H., and Gerard, G., "Elastic Stability of Orthotropic Shells," Jour. Aerospace Sciences, Vol. 29, No. 5, May 1962.

Contrails

Unclassified

Security Classification

DOCUMENT CONTROL DATA - R&D		
(Security classification of title, body of abstract and indexing annotation must be entered when the overall report is classified)		
1. ORIGINATING ACTIVITY (Corporate author) Allied Research Associates, Inc. Virginia Road, Concord, Massachusetts	2a. REPORT SECURITY CLASSIFICATION Unclassified 2b. GROUP	
3. REPORT TITLE GENERAL INSTABILITY OF ORTHOTROPICALLY STIFFENED CYLINDERS PART II - BENDING AND COMBINED COMPRESSION AND BENDING		
4. DESCRIPTIVE NOTES (Type of report and inclusive dates) Final Report		
5. AUTHOR(S) (Last name, first name, initial) Lakshmikantham, C. - Gerard, George - Milligan, Roger		
6. REPORT DATE August 1965	7a. TOTAL NO. OF PAGES 41	7b. NO. OF REFS 5
8a. CONTRACT OR GRANT NO. AF 33(615)-1228 b. PROJECT NO. 1467 c. Task No. 146703 d. BPSN 4(6199-146703-62405334)	8a. ORIGINATOR'S REPORT NUMBER(S) ARA Technical Report No. 258-3 8b. OTHER REPORT NO(S) (Any other numbers that may be assigned this report) Technical Report AFFDL-TR-65-161, Part II	
10. AVAILABILITY/LIMITATION NOTICES The distribution of this report is unlimited.		
11. SUPPLEMENTARY NOTES	12. SPONSORING MILITARY ACTIVITY Air Force Flights Dynamics Laboratory Research and Technology Division Air Force Systems Command - USAF Wright-Patterson AFB, Ohio	
13. ABSTRACT <p>As part of a general program to determine the applicability of linear orthotropic theory to the design of cylindrical shells under various loading conditions, a theoretical and experimental investigation was performed on the general instability of orthotropic cylinders under bending and combined axial compression and bending loading.</p> <p>Based on a simple approximation for the asymmetric buckling pattern, theoretical results suitable for design use were obtained for the buckling of orthotropic cylinders for both bending and combined loading conditions. It was shown that the buckling stress for orthotropic cylinders under bending or axial compression loading are equal which agrees with previous results for isotropic cylinders. Theoretical results were evaluated by means of a series of careful experiments performed on orthotropically stiffened cylinders designed to fail in the elastic general instability mode. For both bending loading and the combined axial and bending loading condition, experimental results were in good agreement with the theory.</p>		

DD FORM 1473
1 JAN 64

Unclassified

Security Classification

Unclassified
Security Classification

14.	KEY WORDS	LINK A		LINK B		LINK C	
		ROLE	WT	ROLE	WT	ROLE	WT
	Stability of Cylindrical Orthotropic Shells Bending Loading Combined Axial Compression and Bending Loading Experimental Results Theoretical Results Stability of Isotropic Cylinders in Bending						

INSTRUCTIONS

1. **ORIGINATING ACTIVITY:** Enter the name and address of the contractor, subcontractor, grantee, Department of Defense activity or other organization (*corporate author*) issuing the report.
- 2a. **REPORT SECURITY CLASSIFICATION:** Enter the overall security classification of the report. Indicate whether "Restricted Data" is included. Marking is to be in accordance with appropriate security regulations.
- 2b. **GROUP:** Automatic downgrading is specified in DoD Directive 5200.10 and Armed Forces Industrial Manual. Enter the group number. Also, when applicable, show that optional markings have been used for Group 3 and Group 4 as authorized.
3. **REPORT TITLE:** Enter the complete report title in all capital letters. Titles in all cases should be unclassified. If a meaningful title cannot be selected without classification, show title classification in all capitals in parenthesis immediately following the title.
4. **DESCRIPTIVE NOTES:** If appropriate, enter the type of report, e.g., interim, progress, summary, annual, or final. Give the inclusive dates when a specific reporting period is covered.
5. **AUTHOR(S):** Enter the name(s) of author(s) as shown on or in the report. Enter last name, first name, middle initial. If military, show rank and branch of service. The name of the principal author is an absolute minimum requirement.
6. **REPORT DATE:** Enter the date of the report as day, month, year, or month, year. If more than one date appears on the report, use date of publication.
- 7a. **TOTAL NUMBER OF PAGES:** The total page count should follow normal pagination procedures, i.e., enter the number of pages containing information.
- 7b. **NUMBER OF REFERENCES:** Enter the total number of references cited in the report.
- 8a. **CONTRACT OR GRANT NUMBER:** If appropriate, enter the applicable number of the contract or grant under which the report was written.
- 8b, 8c, & 8d. **PROJECT NUMBER:** Enter the appropriate military department identification, such as project number, subproject number, system numbers, task number, etc.
- 9a. **ORIGINATOR'S REPORT NUMBER(S):** Enter the official report number by which the document will be identified and controlled by the originating activity. This number must be unique to this report.
- 9b. **OTHER REPORT NUMBER(S):** If the report has been assigned any other report numbers (*either by the originator or by the sponsor*), also enter this number(s).
10. **AVAILABILITY/LIMITATION NOTICES:** Enter any limitations on further dissemination of the report, other than those

imposed by security classification, using standard statements such as:

- (1) "Qualified requesters may obtain copies of this report from DDC."
- (2) "Foreign announcement and dissemination of this report by DDC is not authorized."
- (3) "U. S. Government agencies may obtain copies of this report directly from DDC. Other qualified DDC users shall request through _____."
- (4) "U. S. military agencies may obtain copies of this report directly from DDC. Other qualified users shall request through _____."
- (5) "All distribution of this report is controlled. Qualified DDC users shall request through _____."

If the report has been furnished to the Office of Technical Services, Department of Commerce, for sale to the public, indicate this fact and enter the price, if known.

11. **SUPPLEMENTARY NOTES:** Use for additional explanatory notes.
12. **SPONSORING MILITARY ACTIVITY:** Enter the name of the departmental project office or laboratory sponsoring (*paying for*) the research and development. Include address.
13. **ABSTRACT:** Enter an abstract giving a brief and factual summary of the document indicative of the report, even though it may also appear elsewhere in the body of the technical report. If additional space is required, a continuation sheet shall be attached.

It is highly desirable that the abstract of classified reports be unclassified. Each paragraph of the abstract shall end with an indication of the military security classification of the information in the paragraph, represented as (TS), (S), (C), or (U).

There is no limitation on the length of the abstract. However, the suggested length is from 150 to 225 words.

14. **KEY WORDS:** Key words are technically meaningful terms or short phrases that characterize a report and may be used as index entries for cataloging the report. Key words must be selected so that no security classification is required. Identifiers, such as equipment model designation, trade name, military project code name, geographic location, may be used as key words but will be followed by an indication of technical context. The assignment of links, rules, and weights is optional.

Unclassified
Security Classification